Supplementary Information

Asymmetrically coordinated ZnCoFe hetero-trimetallic atom catalyst enhances electrocatalytic oxygen reaction

Changli Chen[‡a,b], Jing Chai[‡c], Mengru Sun[‡b], Tianqi Guo*[d], Jie Lin[e], Yurong Zhou[d], Zhiyi Sun[b], Fang Zhang[f], Liang Zhang*[c], Wenxing Chen*[b], Yujing Li *[b]

[a.] School of Chemistry and Chemical Engineering, Qilu University of Technology (Shandong Academy of Sciences), Jinan 250353, P. R. China

[b.] Energy & Catalysis Center, School of Materials Science and Engineering, Beijing Institute of Technology, Beijing 100081, China. Email: wxchen@bit.edu.cn, yjli@bit.edu.cn

[c.] Center for Combustion Energy, School of Vehicle and Mobility, State Key Laboratory of Intelligent Green Vehicle and Mobility, Tsinghua University, Beijing 100084, China. Email: zhangbright@tsinghua.edu.cn

[d.] International Iberian Nanotechnology Laboratory (INL), Braga 4715-330, Portugal. Email: tianqi.guo@inl.int

[e.] Ningbo Institute of Materials Technology and Engineering, Chinese Academy of Science Ningbo 315201, China

[f.] Analysis and Testing Center, Beijing Institute of Technology, Beijing Institute of Technology, Beijing 100081, P. R. China.

‡ These authors contributed equally to this work.

Experimental Procedures

Chemicals

Cobalt nitrate hexahydrate (99%, Aladdin), 2-methylimidazole (98%, Innochem), Zinc nitrate hexahydrate (99.5%, Alfa), methanol (99.5%, Sun), $FeCl_3$ (98%, Alfa) and Allyl thiourea (98%, Innochem) were used without any further purification. Ultrapure water (Millipore Milli-Q grade) with a resistivity of 18.2 MΩ was used in all the experiments.

Synthesis of the Zn/NC

$Zn(NO_3)_2 \cdot 6H_2O$ (1.785 g) and 2-methyl imidazole (1.97 g) were added into 50 mL methanol and ultrasound for five minutes respectively. Then, the two solutions were mixed and stirred intensely for 3 min at room temperature. The mixture was kept at 35 ℃ for 6 h. Finally, the precipitant was collected by centrifugation and dried at 80 ℃ in the vacuum oven. The ZIF-8 was obtained after a quick grind. The ZIF-8 was transferred to the tube furnace and s calcined at 1000 ℃ under an inert atmosphere for 3 h with 4 ℃ min^{-1} for the ramp rate of the carbonization process. The Zn/NC was finally obtained after a quick grind.

Synthesis of the ZnCo-DAC/NC

$Zn(NO_3)_2 \cdot 6H_2O$ (1.785 g), $Co(NO_3)_2 \cdot 6H_2O$ (25 mg) and 2-methyl imidazole (1.97 g) were dissolved in 50 mL methanol and ultrasound for five minutes respectively. Then, the two solutions were mixed and stirred intensely for 3 min at room temperature. The mixture was kept at 35 ℃ for 6 h. Finally, the precipitant was collected by centrifugation and dried at 80 ℃ in the vacuum oven. The ZnCo-ZIF was obtained after a quick grind. The ZnCo-ZIF was transferred to the tube furnace and s calcined at 1000 ℃ under an inert atmosphere for 3 h with 4 ℃ min^{-1} for the ramp rate of the carbonization process. The ZnCo-DAC/NC was finally obtained after a quick grind.

Synthesis of the ZnCoFe-TAC/NC

The dried ZnCo-ZIF (0.382 g) were dispersed in 20 mL methanol, then $FeCl_3$ (5 mg) was added to the turbid liquid, and the mixture was stirred intensively for 5 minutes and heated at 80 ℃ for 2 h. After that, the precipitant was collected by centrifugation and dried at 80 ℃ in a vacuum oven. Finally, the powder was calcined at 1000 ℃ under an inert atmosphere for 3 h in a tube furnace with 4 ℃ min^{-1} for the ramp rate of the carbonization process. The ZnCoFe-TAC/NC was finally obtained after a quick grind.

Synthesis of the ZnCoFe-TAC/SNC

The dried ZnCo-ZIF (0.382 g) were dispersed in 20 mL methanol, then $FeCl_3$ (5 mg) and allylthiourea (1 g) were added to the turbid liquid, the mixture was stirred intensively for 5 minutes and heated at 80 ℃ for 2 h. After that, the precipitant was collected by centrifugation and dried at 80 ℃ in a vacuum oven. Eventually, the powder was calcined at 1000 ℃ under an inert atmosphere for 3 h in a tube furnace with 4 ℃ min^{-1} for the ramp rate of the carbonization process. The ZnCoFe-TAC/SNC was finally obtained after a quick grind.

Characterization

The composition and structure of the as-prepared products were characterized by powder X-ray diffraction (XRD), RigakuTTR-III X-ray diffractometer with Cu Kα radiation, λ=1.5418 Å). The morphologies were observed by a scanning electron microscope (SEM, JSM-6700F, 5kV) and a transmission electron microscope (TEM, JEOL JEM-2100F microscope, 200 kV). The HAADF-STEM images and EDS elemental mapping were carried out in a JEOL ARM-200 microscope at 200 kV, equipped with a probe spherical aberration corrector. The samples were dispersed in ethanol

and dropped onto a copper grid with a carbon film coated for TEM characterizations.

XAFS measurements and data processing.

The X-ray absorption find structure spectra data were collected at BL14W1 station in Shanghai Synchrotron Radiation Facility (SSRF, operated at 3.5 GeV with a maximum current of 250 mA), respectively. The data were collected at room temperature (Zn, Co, and Fe K-edge in fluorescence excitation mode using a 7-element Ge detector). All samples were pelletized as disks of 13 mm diameter with 1mm thickness using graphite powder as a binder.

The acquired EXAFS data were processed according to the standard procedures using the Athena and Artemis implemented in the IFEFFIT software packages. The fitting detail is described below: The acquired EXAFS data were processed according to the standard procedures using the ATHENA module implemented in the IFEFFIT software packages. The EXAFS spectra were obtained by subtracting the post-edge background from the overall absorption and then normalizing concerning the edge-jump step. Subsequently, the χ(k) data of Fourier transformed to real (R) space using hanging windows (dk=1.0 $Å^{-1}$) to separate the EXAFS contributions from different coordination shells. To obtain the quantitative structural parameters around central atoms, least-squares curve parameter fitting was performed using the ARTEMIS module of the IFEFFIT software packages.[22] The following EXAFS equation was used:

$$\chi(k) = \sum_j \frac{N_j S_o^2 F_j(k)}{kR_j^2} exp[-2k^2\sigma_j^2] exp[\frac{-2R_j}{\lambda(k)}] sin[2kR_j + \emptyset_j(k)] \quad (1)$$

S_0^2 is the amplitude reduction factor, $F_j(k)$ is the effective curved-wave backscattering amplitude, N_j is the number of neighbors in the j^{th} atomic shell, R_j is the distance between the X-ray absorbing central atom and the atoms in the j^{th} atomic shell (backscatter), λ is the mean free path in Å, $\phi_j(k)$ is the phase shift (including the phase shift for each shell and the total central atom phase shift), σ_j is the Debye-Waller parameter of the j^{th} atomic shell (variation of distances around the average R_j). The functions $F_j(k)$, λ and $\phi_j(k)$ were calculated with the ab initio code FEFF8.2. The additional details for EXAFS simulations are given below.

The coordination numbers of model samples (metal foil) were fixed as the nominal values. The obtained S_0^2 was fixed in the subsequent fitting of metal single-atom samples. While the internal atomic distances R, Debye-Waller factor σ^2, and the edge-energy shift ΔE_0 were allowed to run freely.

Soft-XAS and XPS measurements

The Soft-XAS spectra of C, N K-edge was measured at beamline BL12B of the National Synchrotron Radiation Laboratory (NSRL). The Zn, Co, Fe K-edge XANES spectra of ZnCoFe-TAC/SNC were collected at the BL11A beamline of the National Synchrotron Radiation Research Center (NSRRC). The XANES spectra of S L-edge were recorded at the 4B7A station in Beijing Synchrotron Radiation Facility in TEY mode. The samples were deposited onto double-sided carbon tape for X-ray spectroscopy.

X-ray photoelectron spectroscopy (XPS) spectra were recorded on an AXIS Supra. The binding energies obtained in the X-ray photoelectron spectral analysis were corrected by the C1s to 284.8 eV (standard peak of contaminated carbon).

***In-situ* XAFS measurements**

A catalyst-modified carbon paper was used as the working electrode, graphite rod as the counter electrode and Ag/AgCl (KCl-saturated) electrode as the reference electrode. A home-made

electrochemical cell was used for *in-situ* XAFS measurements. The experiments were performed at the BL1W1B station in BSRF.

Electrochemical measurements

The ORR and OER electrocatalytic activities of the obtained materials were assessed in a standard three-electrode system (with 0.1 M KOH electrolyte) using a Corrtest workstation. A glassy carbon disk modified by the catalyst was used as the working electrode, Hg/HgO(1 KOH) was used as the reference electrode and a platinum net was used as the counter electrode. The preparation of the working electrode: 3 mg of black catalyst was dispersed into 500 μL of solution (with 490 μL of ethanol and 10 μL of Nafion) to form homogeneous black ink after sufficient ultrasonic, and then 10 μL of ink was dropped onto the glassy carbon electrode.

Linear sweep voltammogram (LSV) curves were obtained at a scan rate of 5 mV s^{-1} after conducting fifty cyclic voltammograms at a scan rate of 200 mV s^{-1} in O_2-saturated 0.1 M KOH. The LSV curves tested in N_2-saturated 0.1 M KOH were used to deduct the background current. All of the current densities have been normalized to the electrode surface area.

The catalytic kinetics were studied by Koutecky-Levich (K-L) analysis. The number of electrons transferred per O_2 molecule (n) was calculated by the K-L equation given below:

$$\frac{1}{j}=\frac{1}{j_k}+\frac{1}{j_d}=-\frac{1}{nFkc_{O_2}^{b}}-\frac{1}{0.62nFAD_{O_2}^{2/3}v^{-1/6}\omega^{1/2}c_{O_2}^{b}} \quad (2)$$

wherein J, J_k and J_d are the experimentally measured current, the kinetic and diffusion-limited currents, respectively, F is the Faraday constant, k is the electrochemical rate constant for O_2 reduction (cm s^{-1}), c is the concentration of O_2, A is the geometric electrode area, D is the diffusion coefficient of O_2, ω and υ are the electrode rotation rate (rad s^{-1}) and the kinematic viscosity, respectively.

The stability of the catalysts was tested by the chronoamperometry (i-t test) and accelerated degradation test (ADT), respectively. The i-t tests were conducted at the potential of 0.5 V, the test time was more than 30000 s. The ADT was measured by CV test, the LSV curve was collected to compared the activity before and after 5000 CV cycles. Besides, the CV curves at 1, 1000, 2000, 3000, 4000 and 5000 cycles were also collected to compare the activity changes of the catalysts.

Zn-air battery assembly and test

A homemade Zn-air battery was constructed. The air cathode was prepared by coating the catalyst on carbon paper with a loading of 1 mg cm^{-2}. A polished Zn plate was employed as an anode and the void between the two electrodes was filled with 6 M KOH and 0.2 M $Zn(AC)_2$. The polarization curves were performed by LSV with 5 mV s^{-1} at 25 ℃ with the electrochemical working station. For the durability test, the electrolyte solution was replaced twice to keep the electrolyte fresh. The test was briefly stopped while the electrolyte was being replaced.

The detail of DFT calculations

In this work, the spin-polarized DFT calculations were carried out in the Vienna Ab Initio simulation package (VASP) in combination with the Atomic Simulation Environment (ASE).[1, 2] The generalized gradient approximation with the Perdew-Burke-Ernzernhof (PBE) functional was used to describe exchange and correlation effects.[3, 4] The electron-ion interaction was described using the projector augmented wave pseudo-potential with the Kohn-Sham plane-wave cutoff energy of 400eV. The Brillouin zone was sampled using the Monkhorst-Pack scheme with a 1×3×1 k-point grid for geometry optimization and a 5×7×1 k-point grid for electronic structure calculation. For the

calculating model, a $4\sqrt{3} \times 8$ orthogonal supercell of CoZnFe was constructed (Fig. S27).[5] The convergence threshold for the forces change was set to be < 0.025 eV/A. A vacuum space of > 15 Å also is used to ensure no appreciable interaction between periodic images. Besides, the Lobster program was used for COHP electronic structure analysis.[6-8]

The OER and ORR mechanisms were considered following the four steps of electrochemical reaction. And the OER mechanism can be written as:

$$OH^- + * \rightarrow OH^* + e^- \quad (3)$$

$$OH^* + OH^- \rightarrow H_2O + O^* + e^- \quad (4)$$

$$O^* + OH^- \rightarrow OOH^* + e^- \quad (5)$$

$$OOH^* + OH^- \rightarrow H_2O + O_2 + e^- \quad (6)$$

where the * stands for an active site, the OH*, O*, and OOH* represent the adsorption intermediates in the reaction process. The ORR is the reverse reaction of OER. The $\triangle G_1$, $\triangle G_2$, $\triangle G_3$, and $\triangle G_4$ are defined as the following. The overpotential of OER and ORR can be described by Equation (11) and Equation (12).

$$\Delta G_1 = \Delta G_{OH^*} - eU \quad (7)$$

$$\Delta G_2 = \Delta G_{O^*} - \Delta G_{OH^*} - eU \quad (8)$$

$$\Delta G_3 = \Delta G_{OOH^*} - \Delta G_{O^*} - eU \quad (9)$$

$$\Delta G_4 = 4.92 - \Delta G_{OOH^*} - eU \quad (10)$$

$$\eta^{OER} = \max\{\Delta G_1, \Delta G_2, \Delta G_3, \Delta G_4\}/e - 1.23\ V \quad (11)$$

$$\eta^{ORR} = 1.23 - \min\{\Delta G_1, \Delta G_2, \Delta G_3, \Delta G_4\}/e \quad (12)$$

During data processing, we used the TS and ZPE to correct the adsorption energy of different intermediates to gain Gibbs free energy (Table S6).

Figures

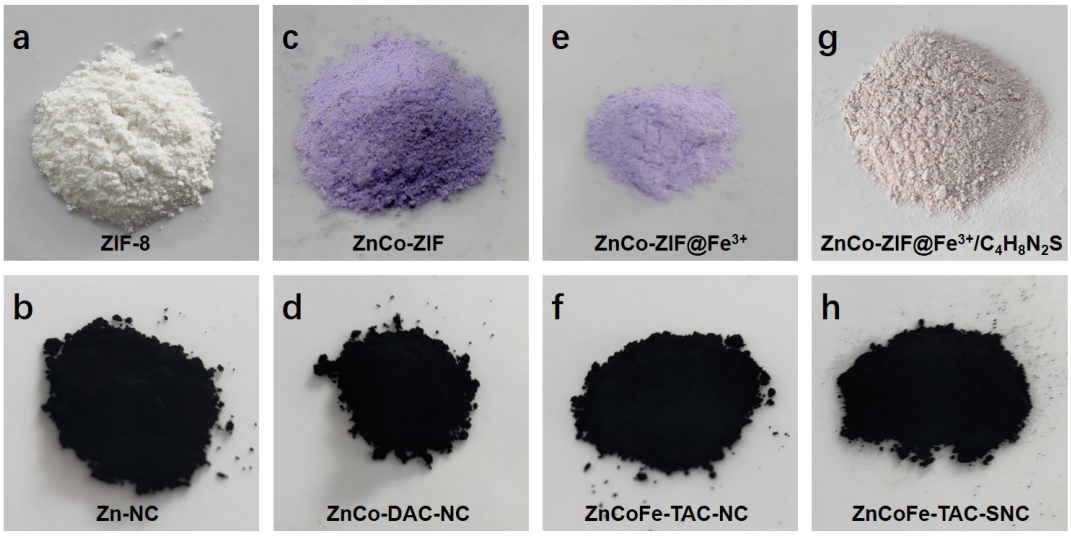

Fig. S1 Digital photographs of the obtained catalysts.

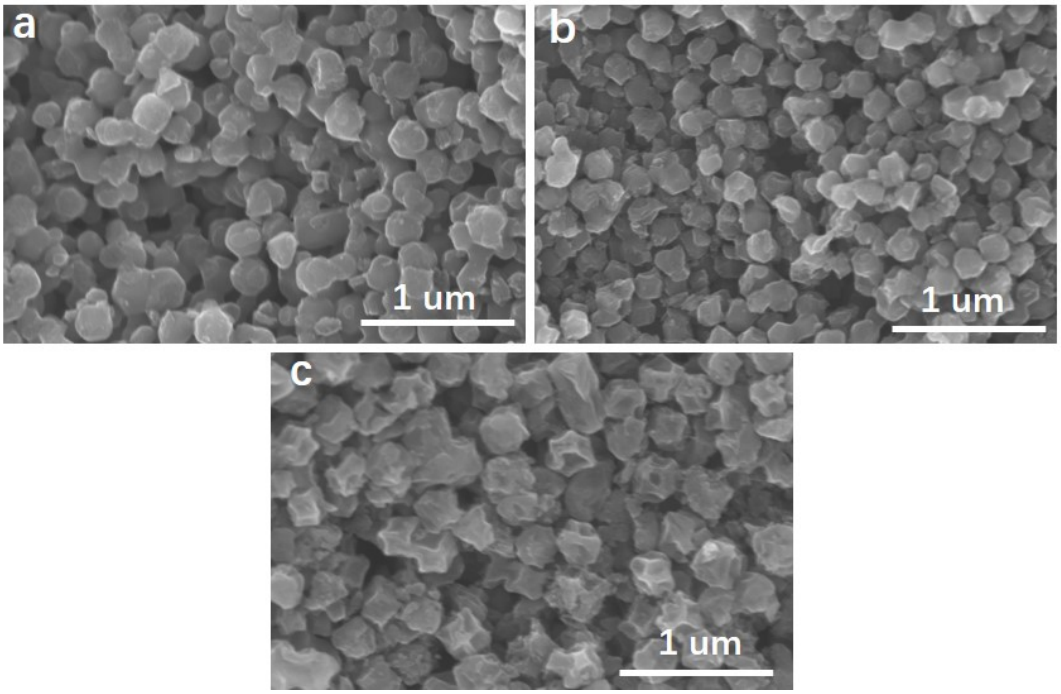

Fig. S2 SEM images of (a) Zn/NC, (b) ZnCo-DAC/NC and (c) ZnCoFe-TAC/NC, respectively.

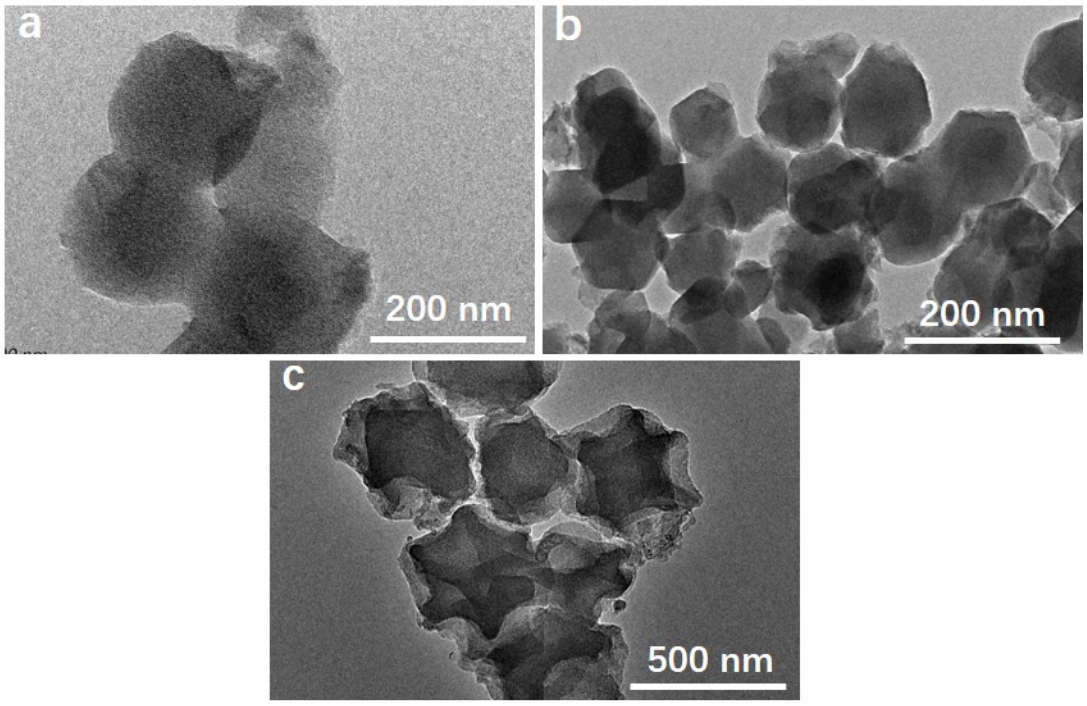

Fig. S3 TEM images of (a) Zn/NC, (b) ZnCo-DAC/NC and (c) ZnCoFe-TAC/NC, respectively.

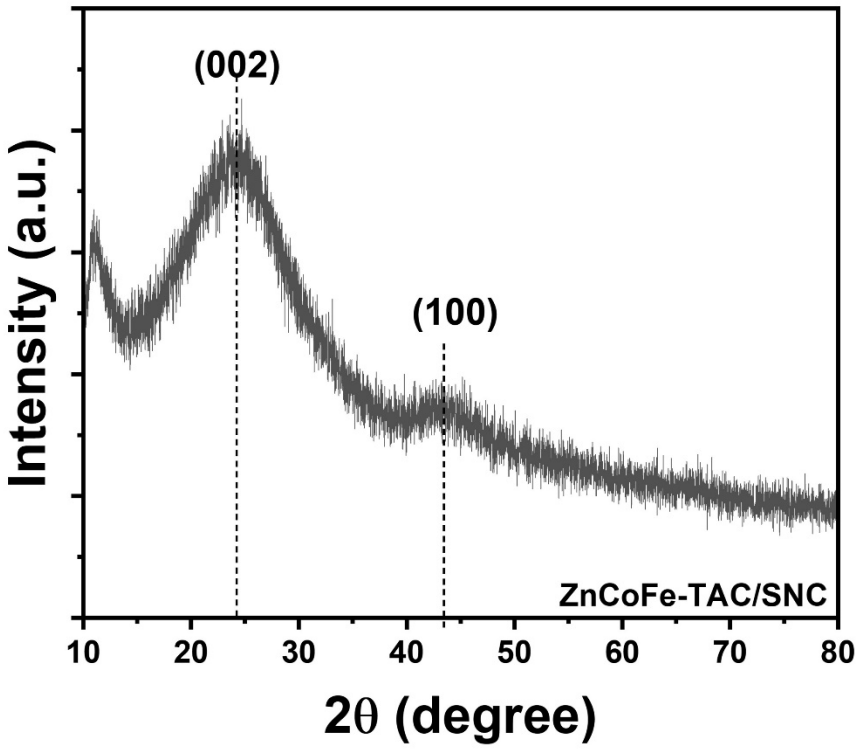

Fig. S4 The XRD pattern of ZnCoFe-TAC/SNC.

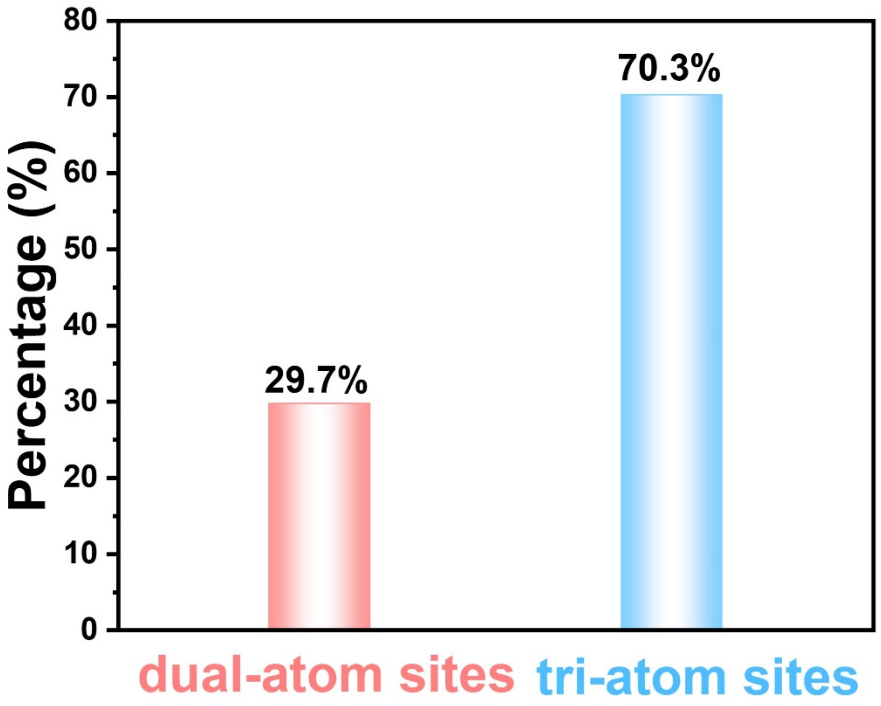

Fig. S5 The diagram for the percentages of dual-metal atom site and trimetallic atom site of ZnCoFe-TAC/SNC.

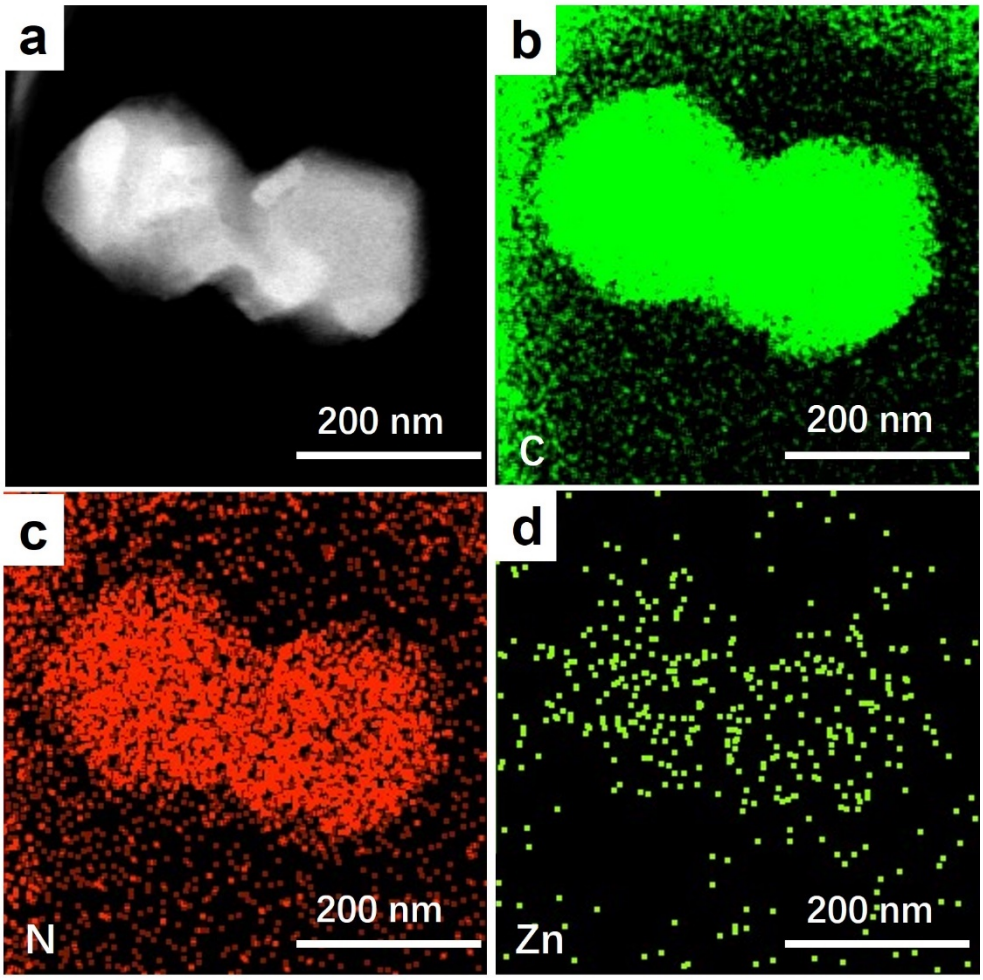

Fig. S6 HAADF-STEM image and the corresponding EDS element maps display the uniform distribution of C (green), N (red) and Zn (peak green) of Zn/NC.

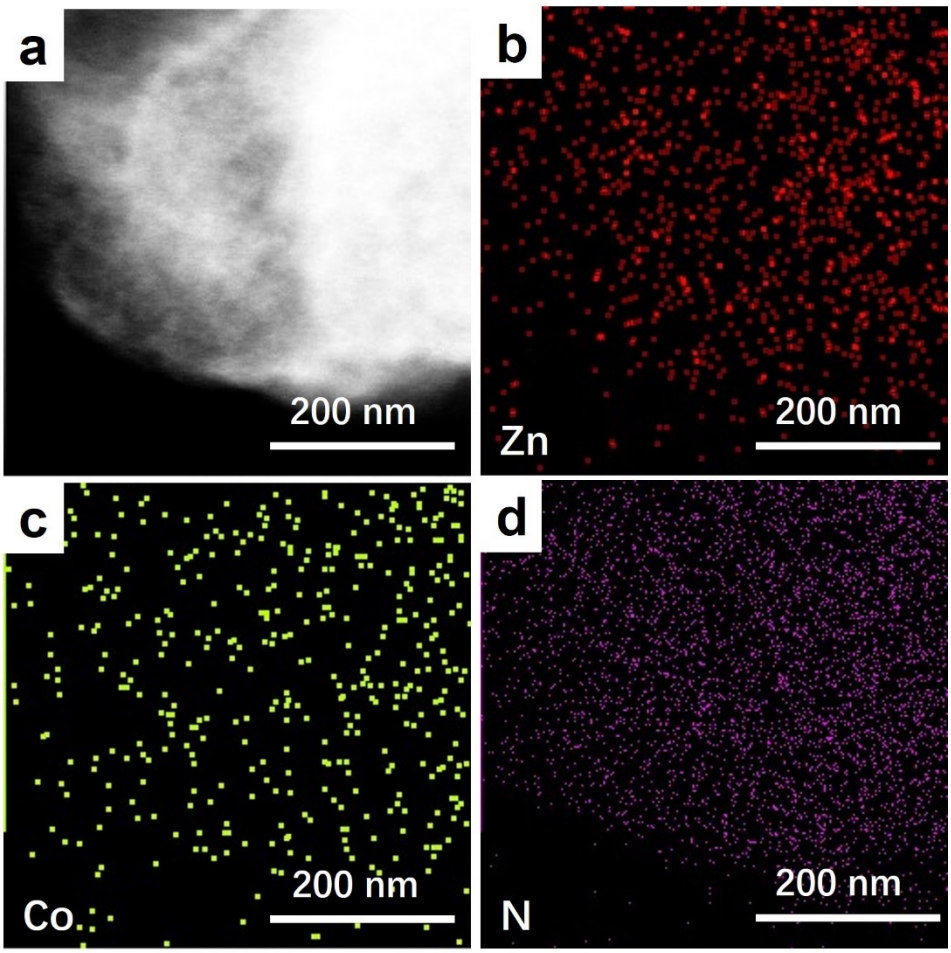

Fig. S7 HAADF-STEM image of ZnCo/NC and the corresponding EDS element maps display the uniform distribution of Zn (red), Co (yellow) and N (purple) of ZnCo/NC.

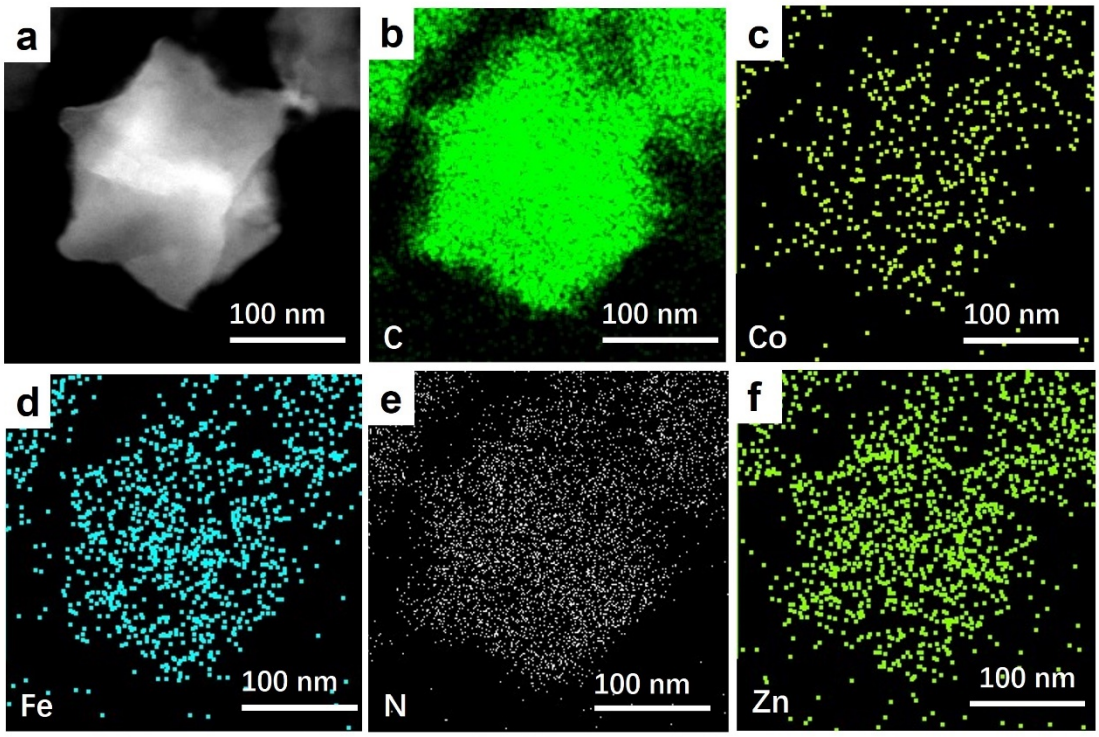

Fig. S8 HAADF-STEM image of ZnCoFe-TAC/NC and the corresponding EDS element maps display the uniform distribution of C (green), Co (kelly), Fe (blue), N (white) and Zn (peak green) of ZnCoFe-TAC/NC.

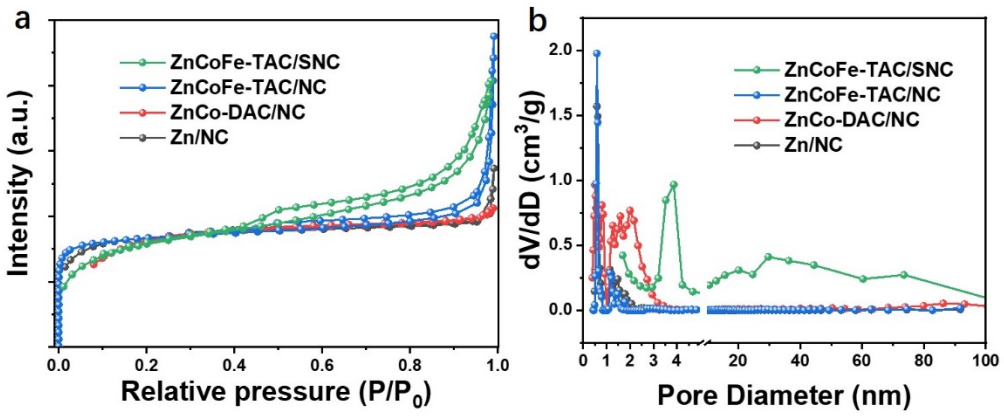

Fig. S9 (a) The nitrogen adsorption/desorption isotherm and (b) pore-size distributions of Zn/NC, ZnCo-DAC/NC, ZnCoFe-TAC/NC and ZnCoFe-TAC/SNC, respectively.

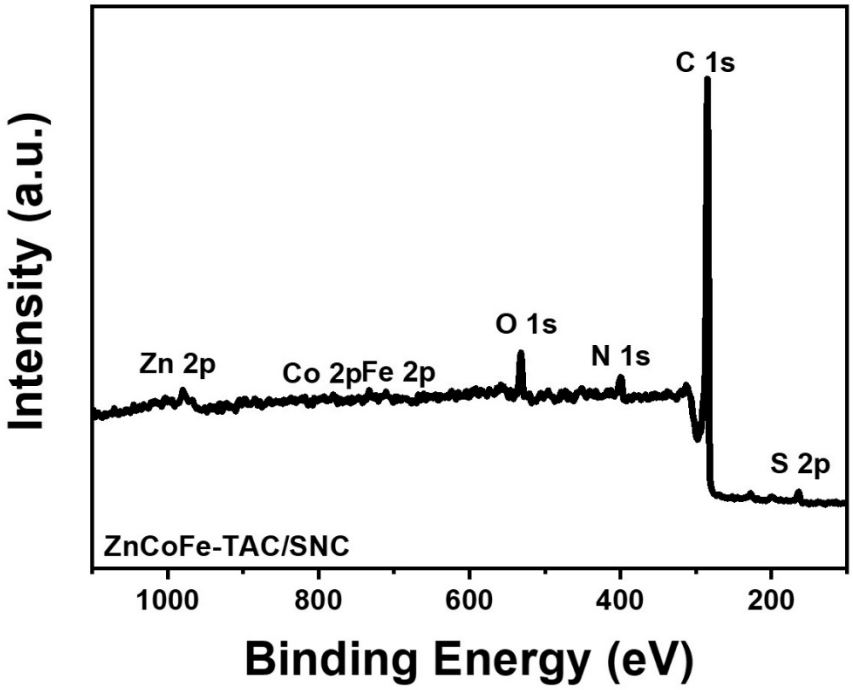

Fig. S10 Wide XPS spectrum of ZnCoFe-TAC/SNC.

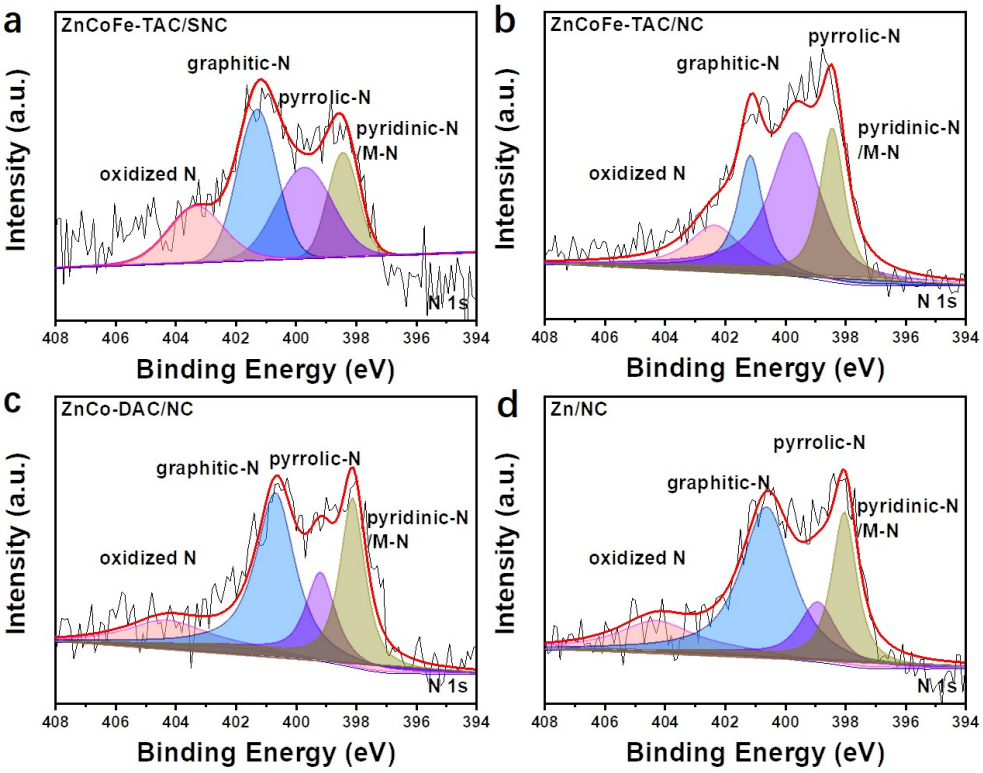

Fig. S11 The N 1s XPS spectrum of (a) ZnCoFe-TAC/SNC, (b) ZnCoFe-TAC/NC, (c) ZnCo-DAC/NC and (d) Zn/NC, respectively.

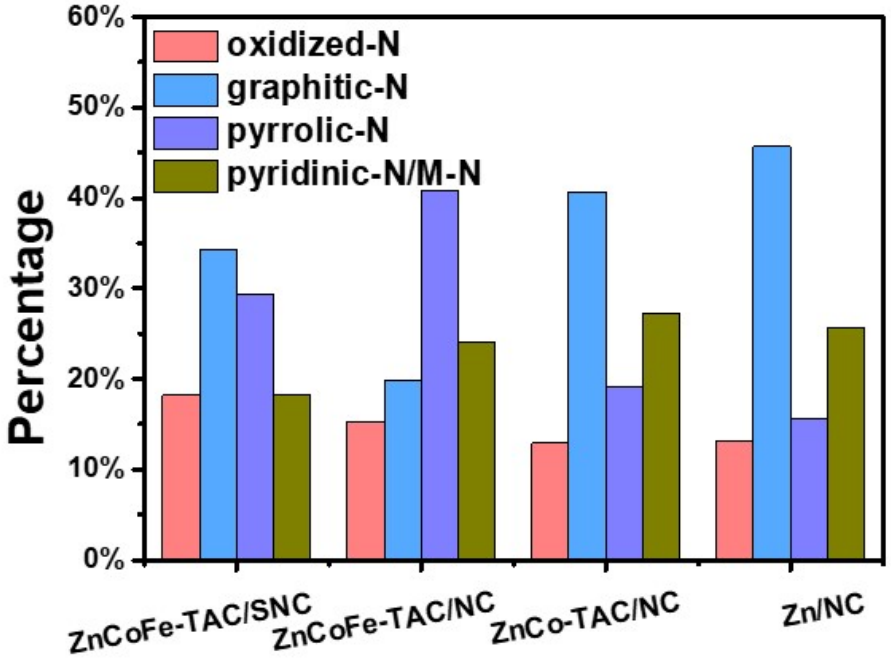

Fig. S12 The area ratio of the four N species, wherein the M-N is the metal-N specie.

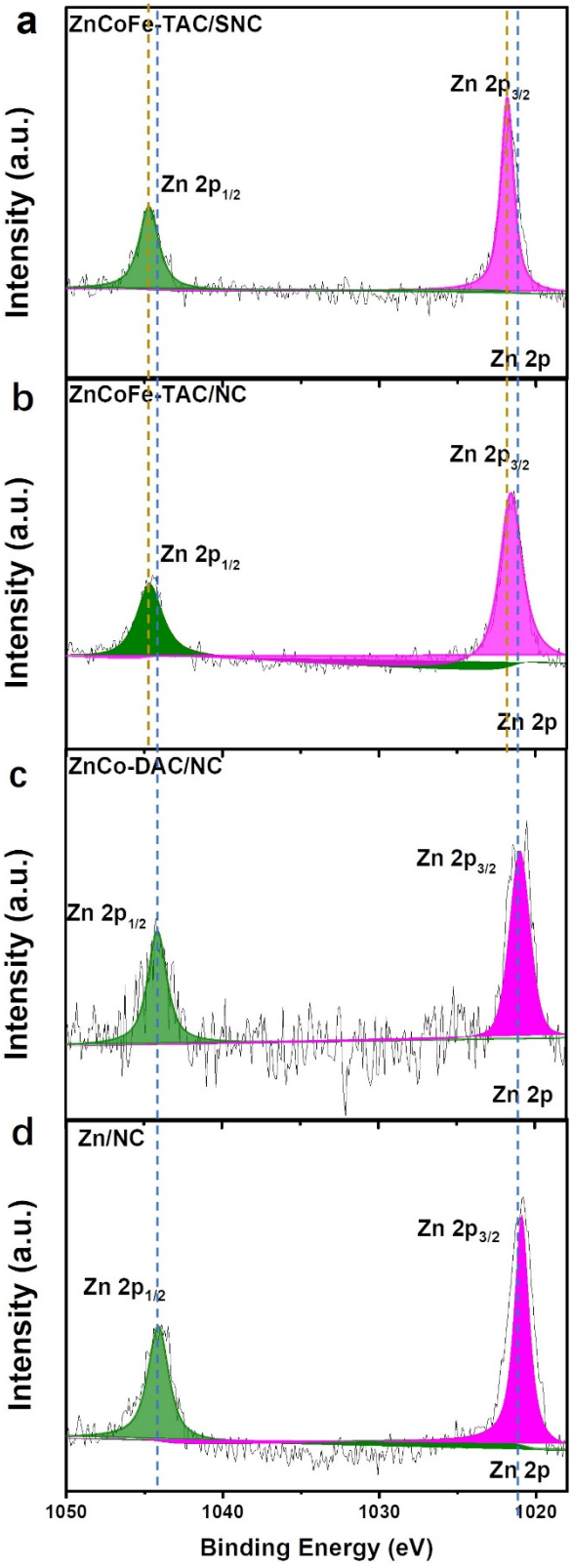

Fig. S13 The XPS spectra of Zn 2p of (a) ZnCoFe-TAC/SNC, (b) ZnCoFe-TAC/NC, (c) ZnCo-DAC/NC and (d) Zn/NC, respectively.

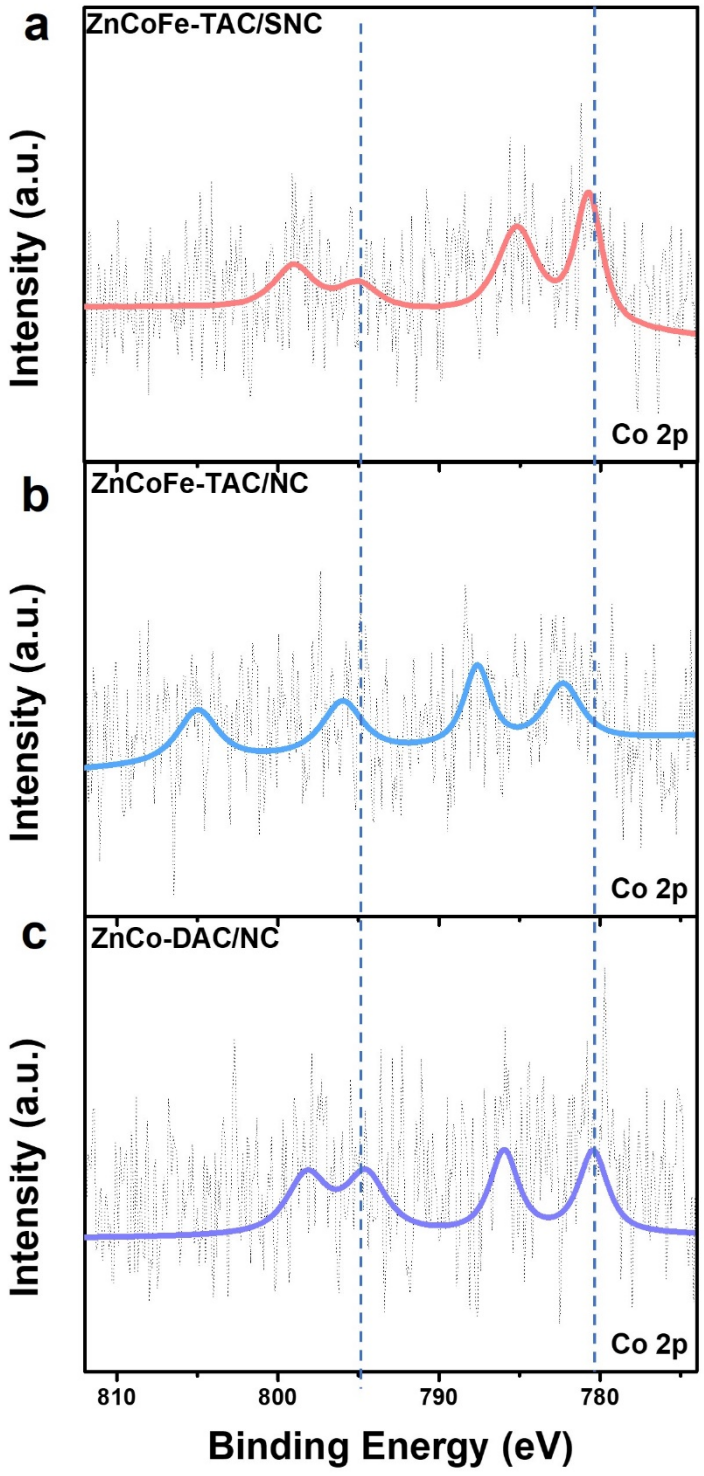

Fig. S14 The XPS spectra of Co 2p of (a) ZnCoFe-TAC/SNC, (b) ZnCoFe-TAC/NC and (c) ZnCo-DAC/NC, respectively.

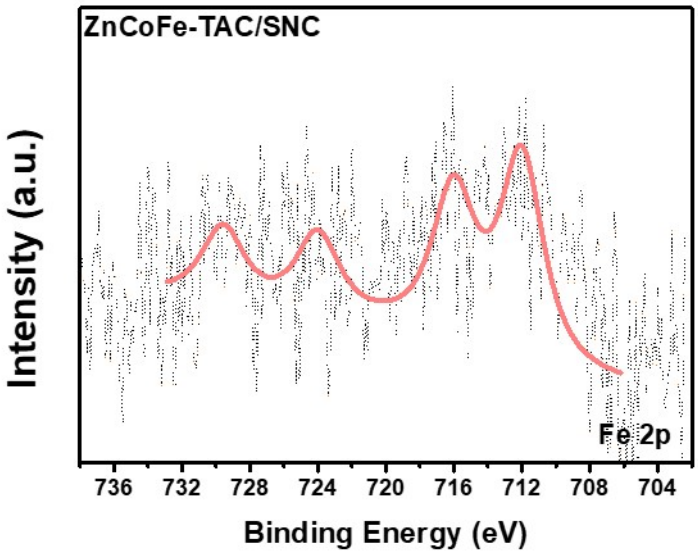

Fig. S15 The XPS spectra of Fe 2p for ZnCoFe-TAC/SNC.

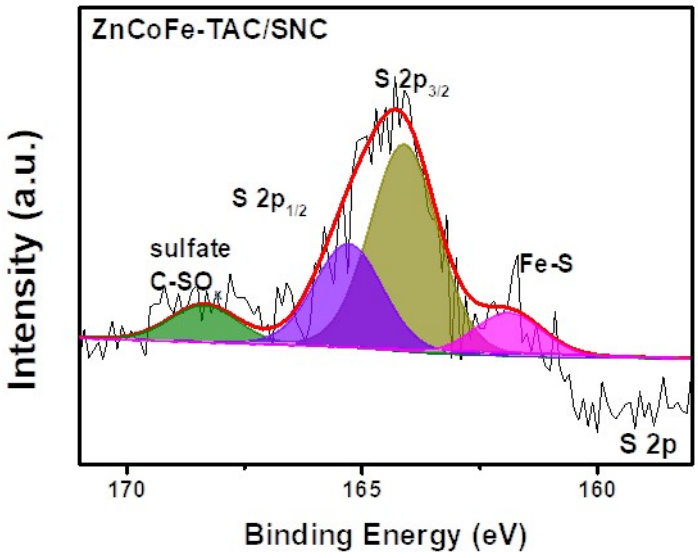

Fig. S16 The XPS spectra of S 2p for of ZnCoFe-TAC/SNC.

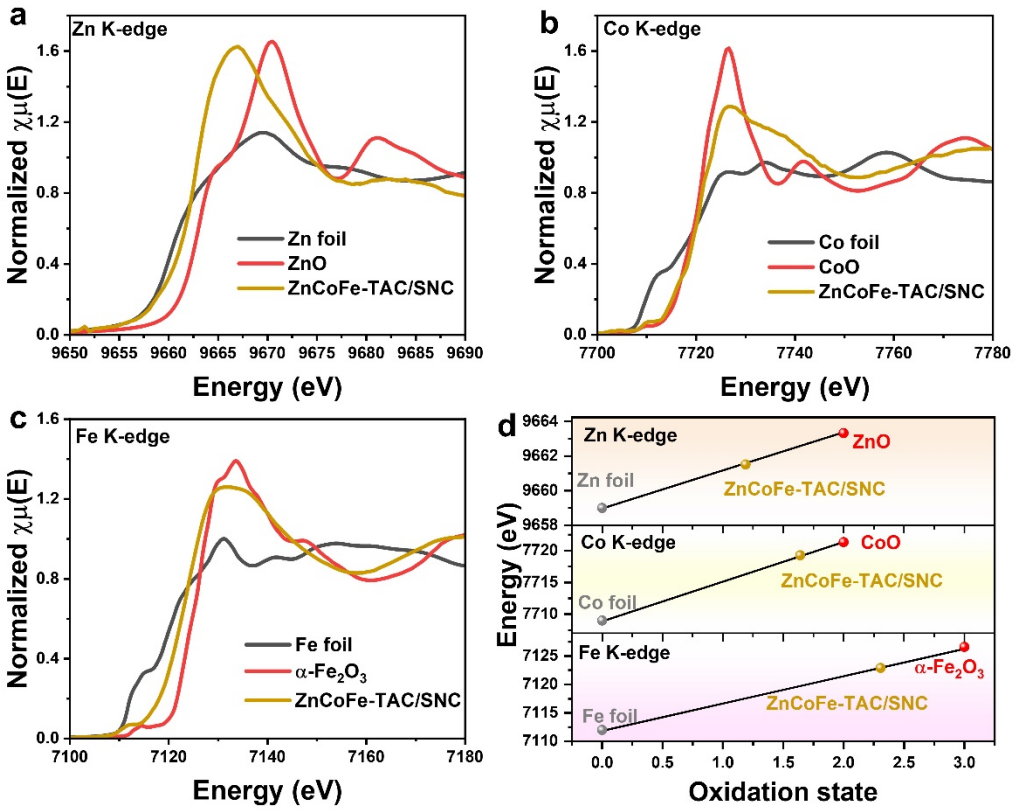

Fig. S17 (a) The experimental Zn K-edge XANES spectra of Zn-TAC and the references (Zn foil, ZnS and ZnPc). (b) The experimental Co K-edge XANES spectra of Co-TAC and the references (Co foil, CoS and CoPc). (c) The experimental Fe K-edge XANES spectra of Fe-TAC and the references (Fe foil, FeS_2 and FePc). (d) Oxidation state of ZnCoFe-TAC/SNC at Zn, Co and Fe K-edge.

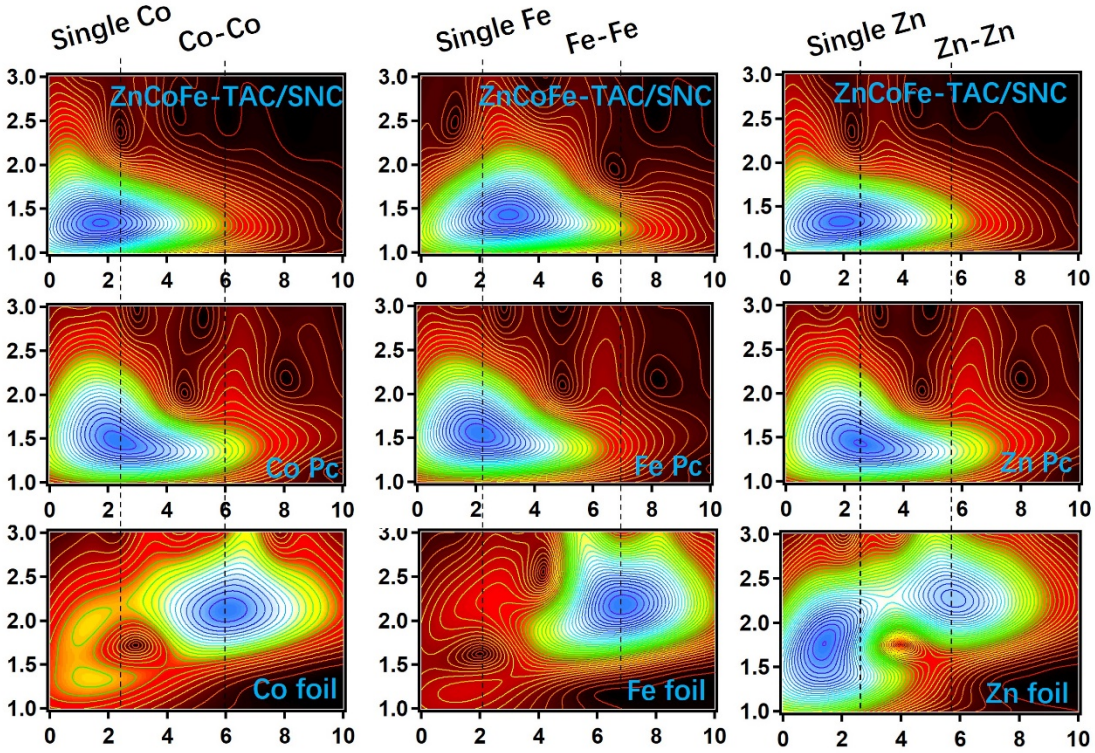

Fig. S18 The wavelet-transform images of Co, Fe and Zn k-edge in ZnCoFe-TAC/SNC and the reference materials, respectively.

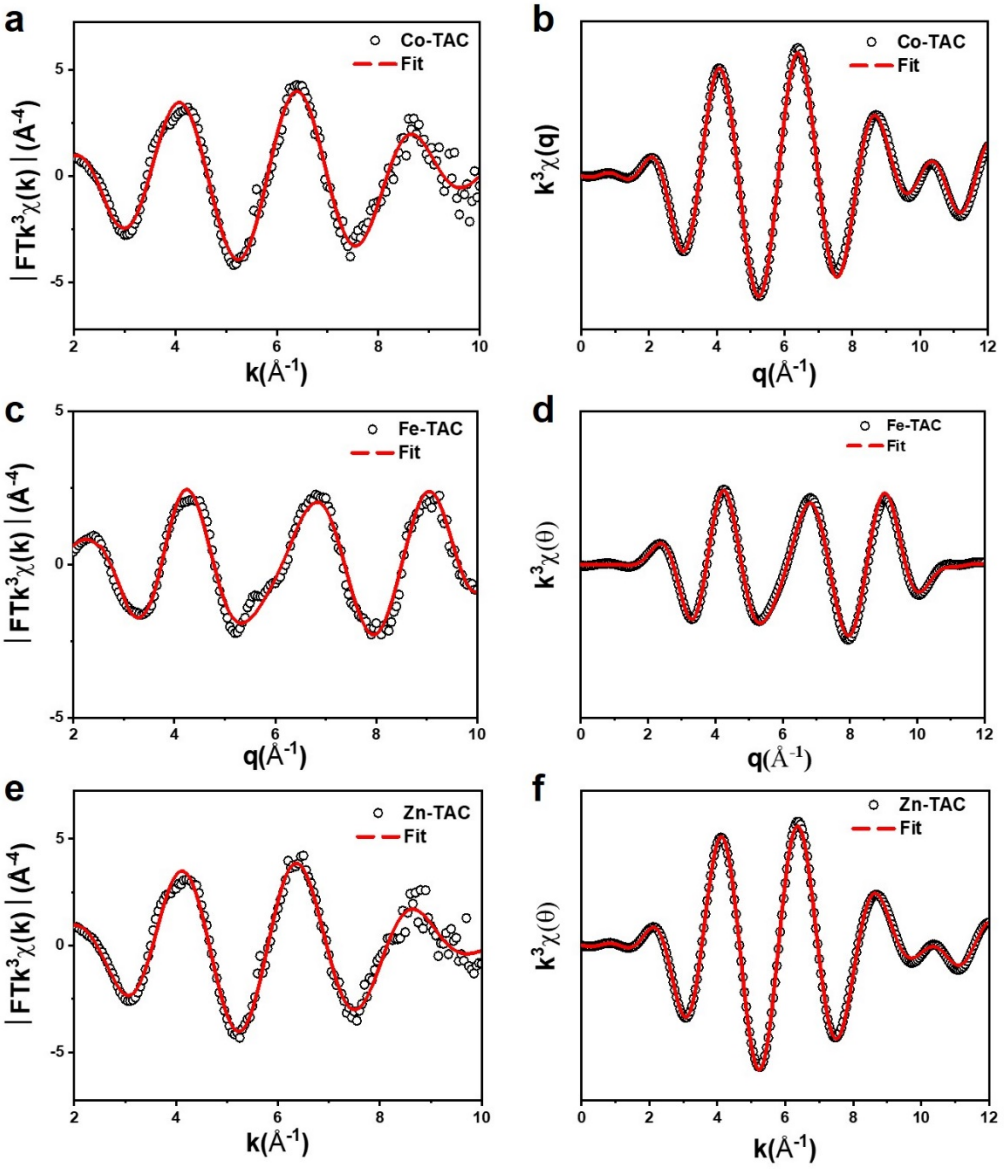

Fig. S19 The k^3-weighted EXAFS in *K*-space and *q*-space for Co, Fe and Zn of ZnCoFe-TAC/SNC, respectively.

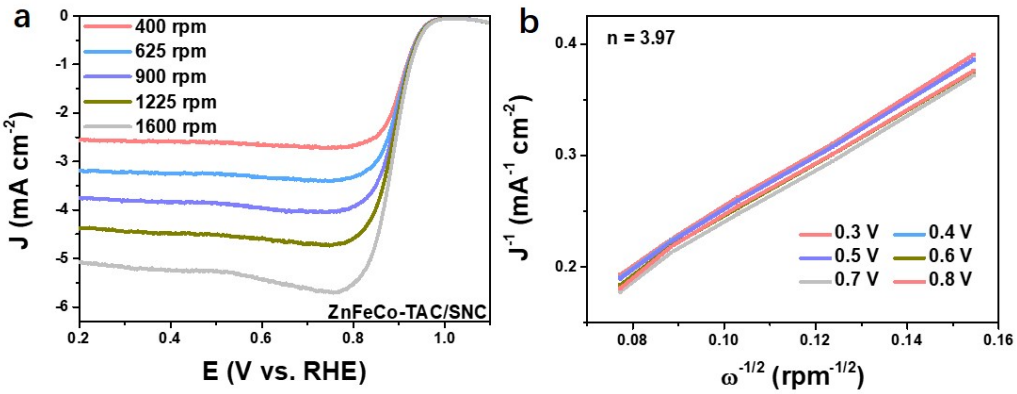

Fig. S20 (a) The LSV curves at various rotating speeds and the (b) K-L plots of ZnCoFe-TAC/SNC.

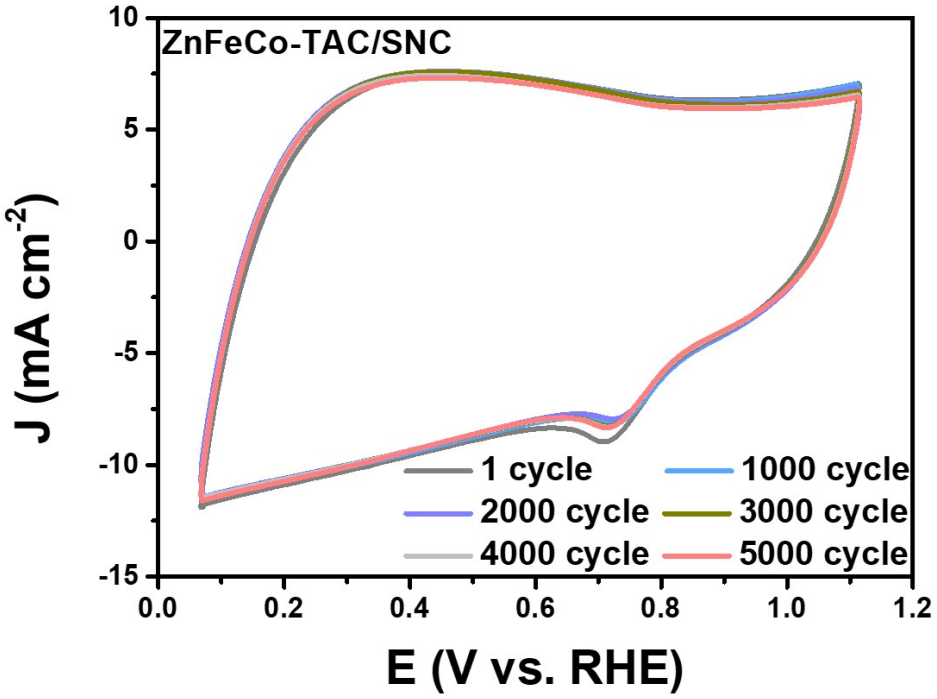

Fig. S21 The CVs of ZnCoFe-TAC/SNC after accelerated degradation test at various cycles.

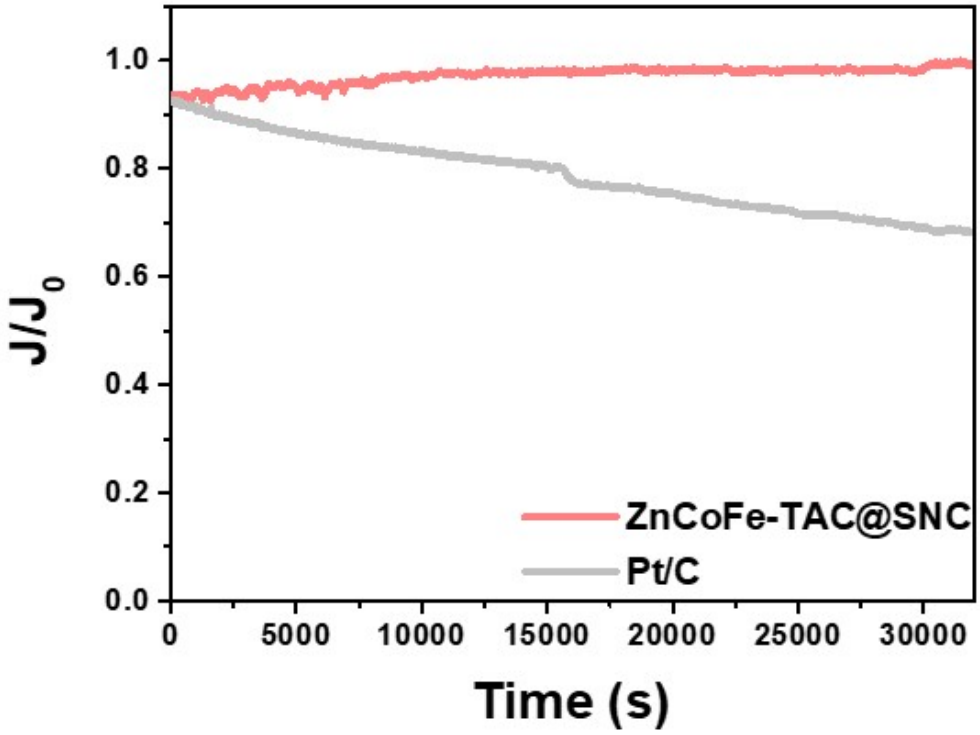

Fig. S22 The i-t curves for ORR stability at 0.5 V.

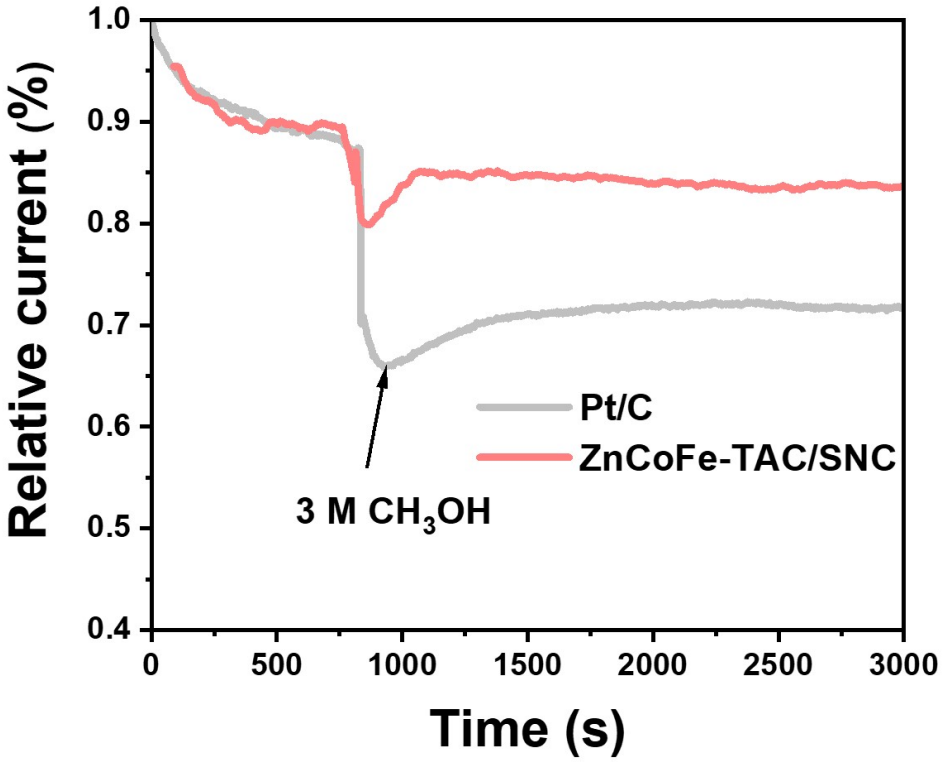

Fig. S23 The curves of methanol resistance test.

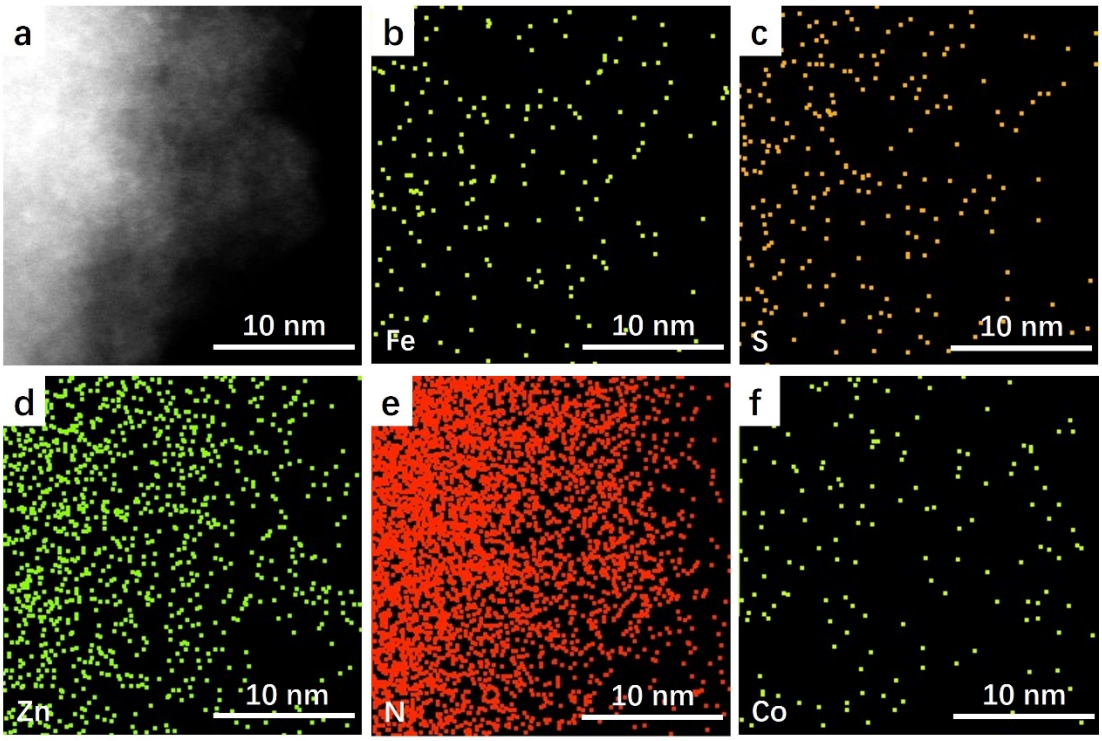

Fig. S24 Characterization of ZnCoFe-TAC/SNC after 5000 CV: (a) HAADF-STEM image of ZnCoFe-TAC/NC shows a solid morphology; (b-f) The corresponding EDS element maps display the uniform distribution of Fe (light green), S (orange), Zn (green), N (red) and Co (peak green) of ZnCoFe-TAC/NC.

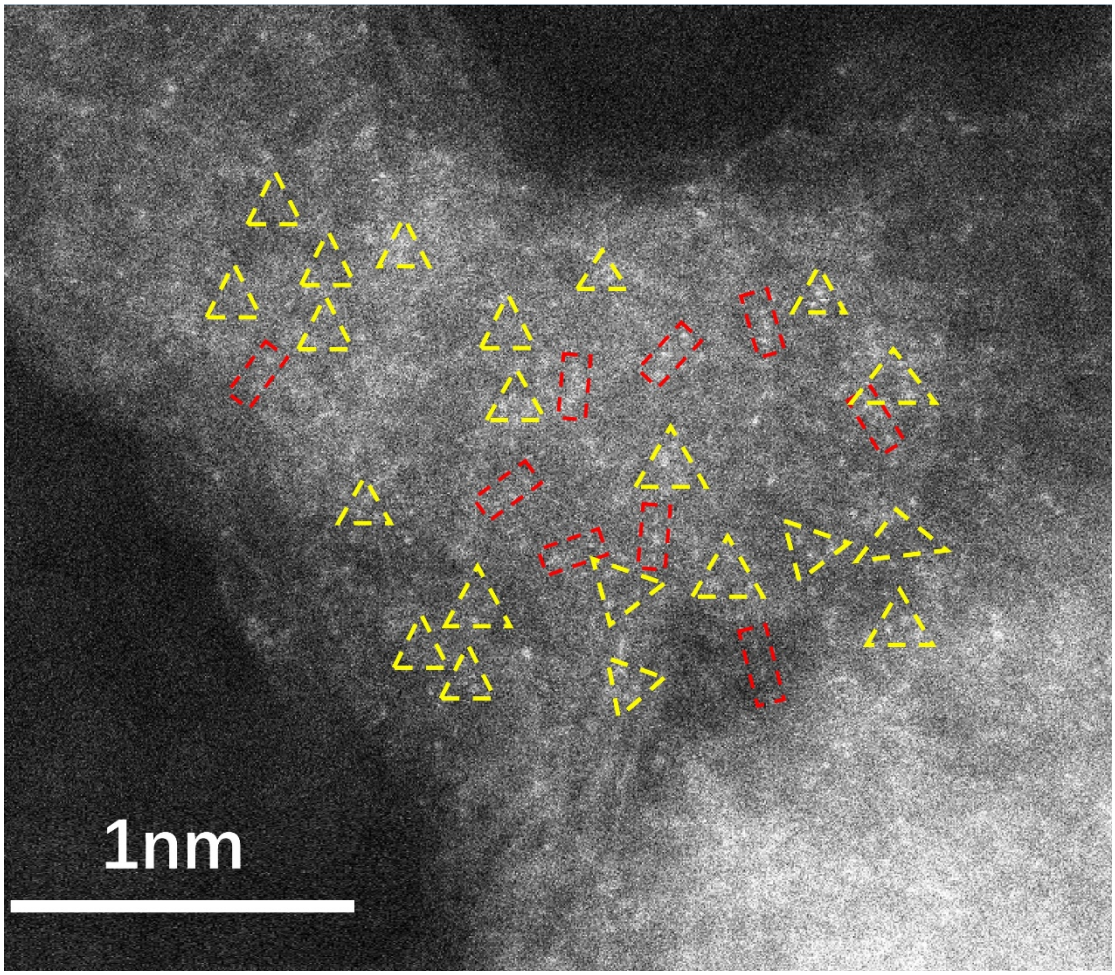

Fig. S25 Characterization of ZnCoFe-TAC/SNC after 5000 CV: Enlarged image of ZnCoFe-TAC/SNC catalyst.

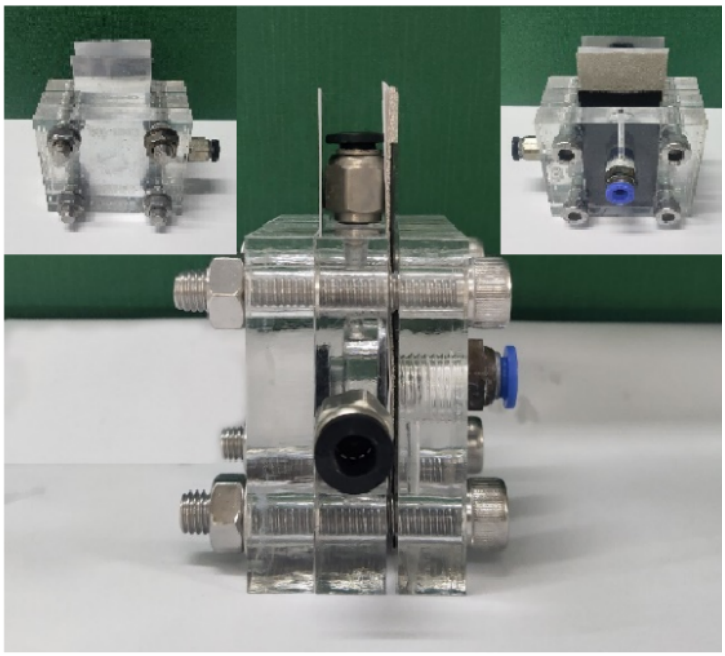

Fig. S26 The homemade rechargeable Zn-air battery.

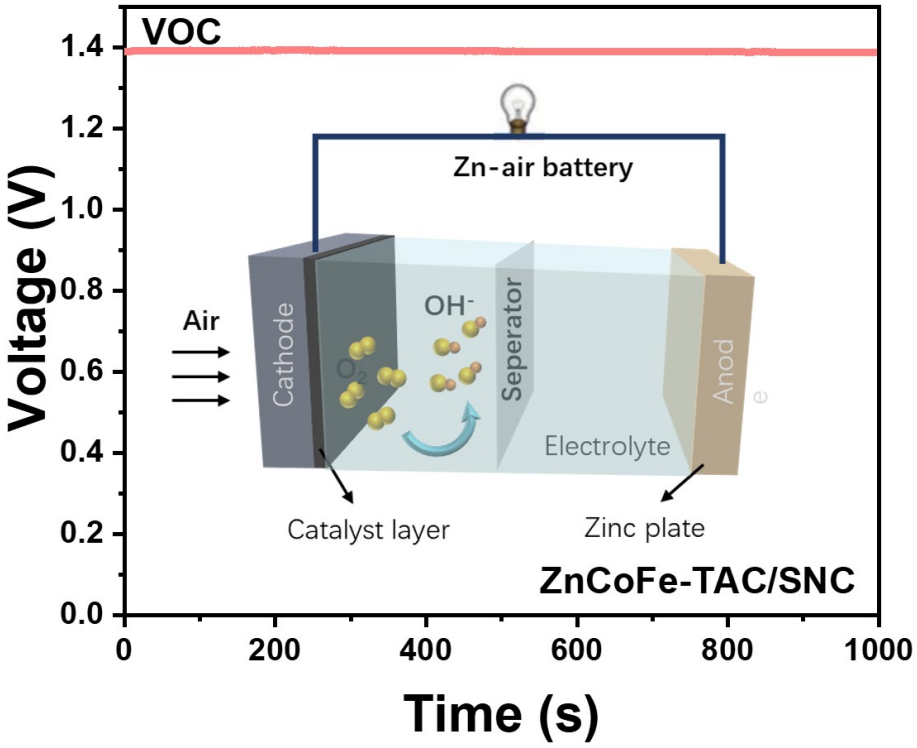

Fig. S27 The open circuit voltage curve (the inset picture is the schematic diagram of Zn-air battery).

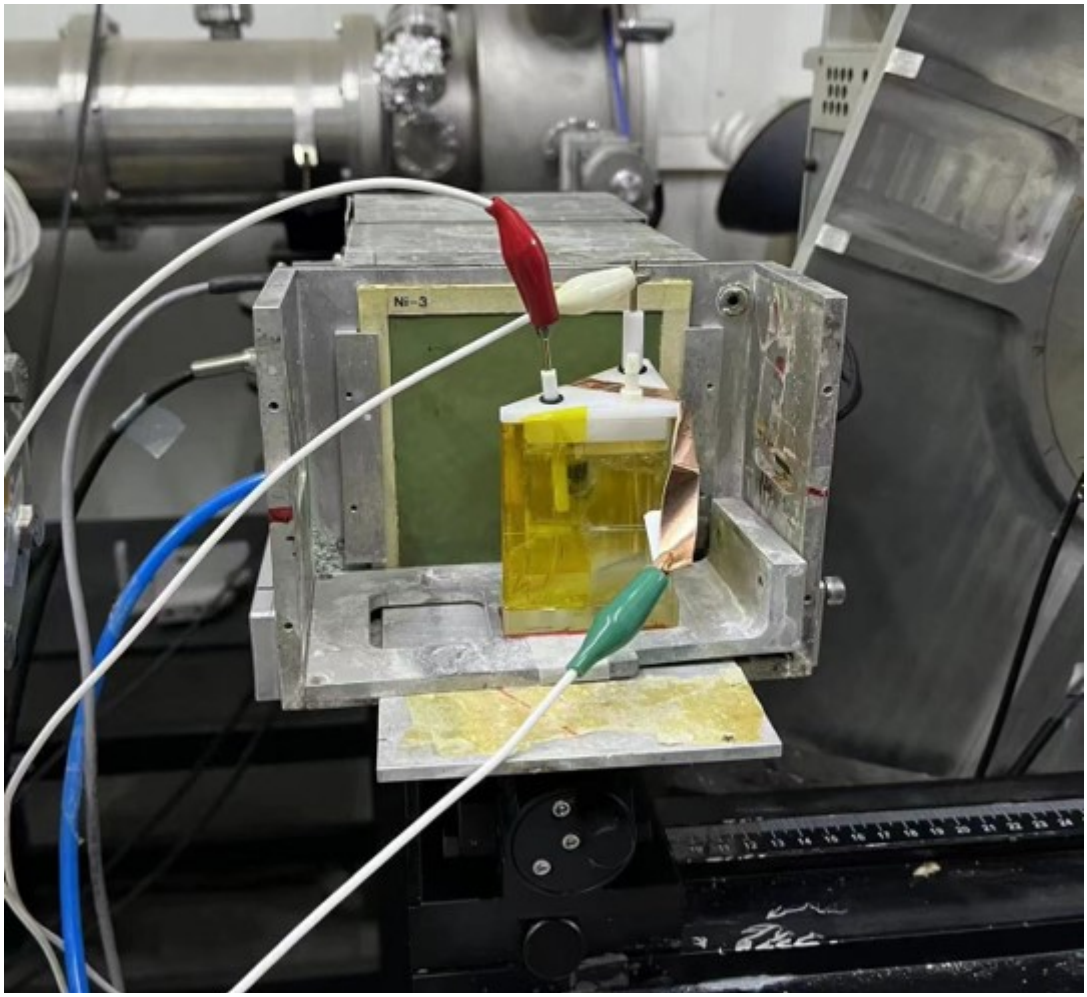

Fig. S28 The photo-diagram of the *in-situ* electrochemical XAS measurements.

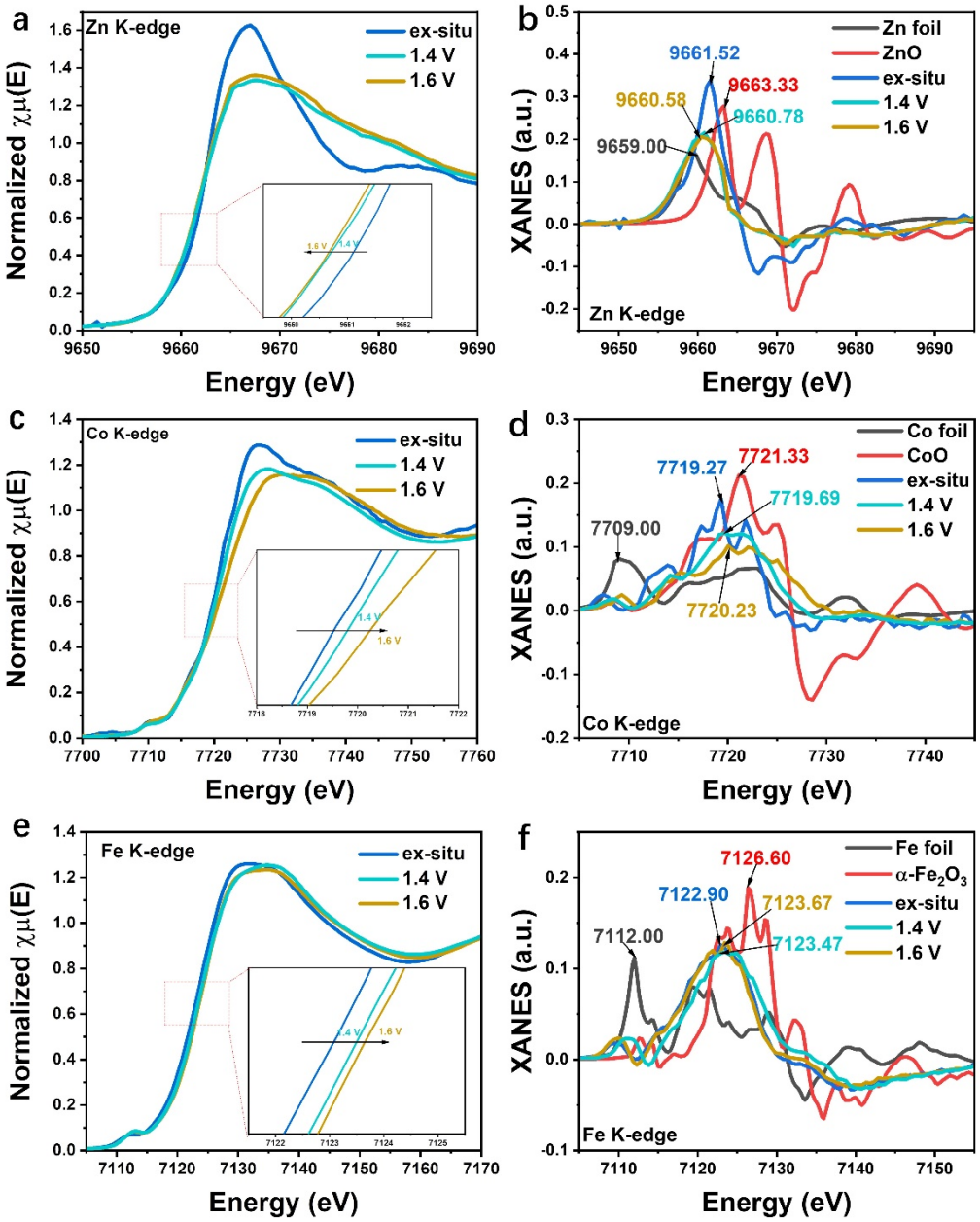

Fig. S29 (a) Normalized XANES spectra at the Zn K-edge. The insets are the magnified image of the near-edge region. (b) Corresponding first-derivative XANES curves at the Zn K-edge. (c) Normalized XANES spectra at the Co K-edge. The insets are the magnified image of the near-edge region. (d) Corresponding first-derivative XANES curves at the Co K-edge. (e) Normalized XANES spectra at the Zn K-edge. The insets are the magnified image of the near-edge region. (f) Corresponding first-derivative XANES curves at the Zn K-edge.

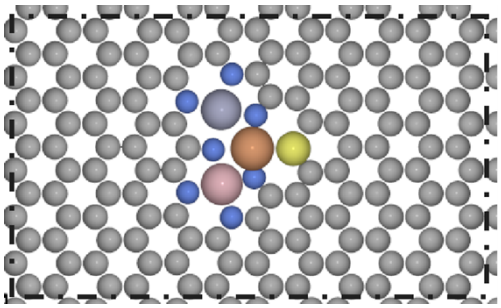

Fig. S30 The configuration of ZnCoFe.

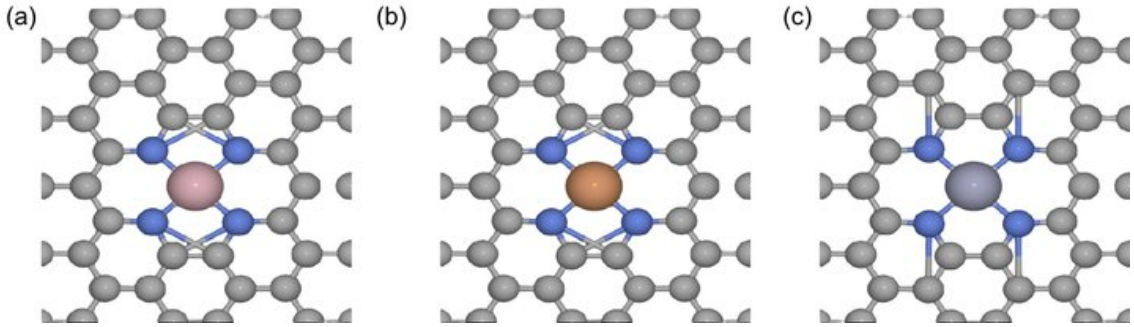

Fig. S31 The calculated structures: (a) CoN_4, (b) FeN_4, (c) ZnN_4. The pink, brown, silver, blue, and grey balls represent the Co, Fe, Zn, N, and C atoms respectively.

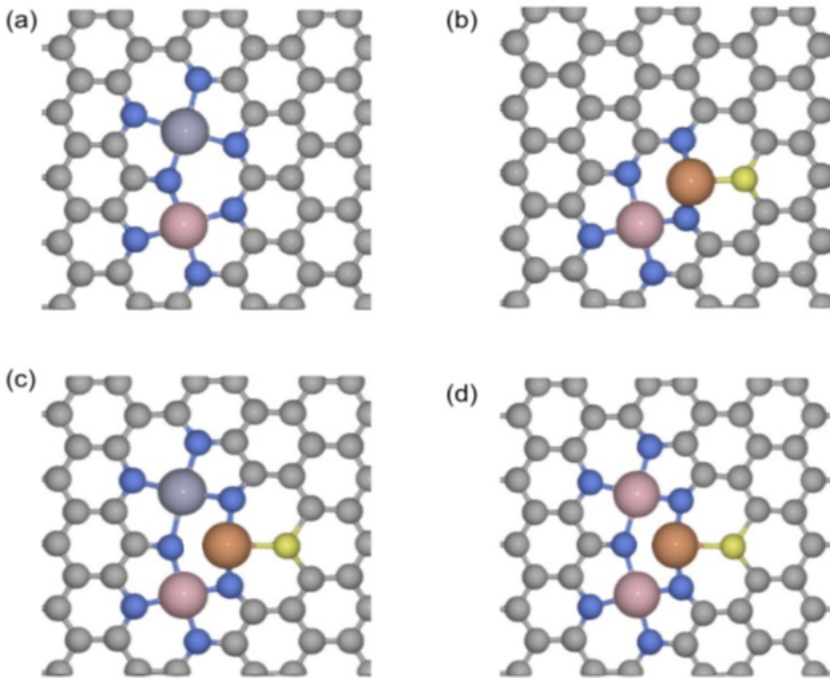

Fig. S32 The calculated structures: (a) CoZn, (b) CoFe, (c)CoZnFe, (d) CoCoFe. The pink, brown, silver, blue, and grey balls represent the Co, Fe, Zn, N, and C atoms respectively.

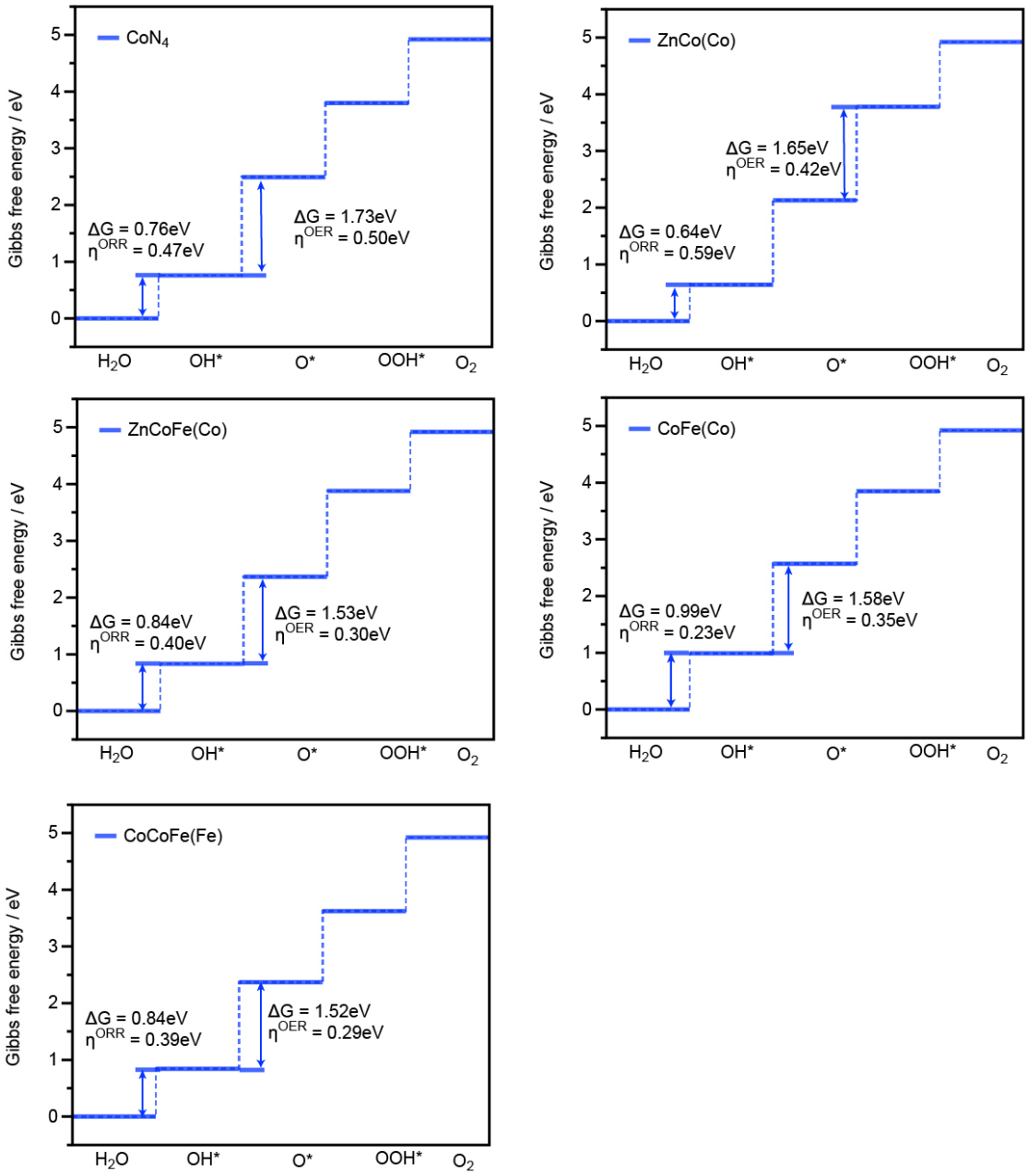

Fig. S33 The free energy diagram (Co as the active site): (a) CoN_4, (b) CoZn, (c) CoZnFe, (d) CoFe, and (e) CoCoFe.

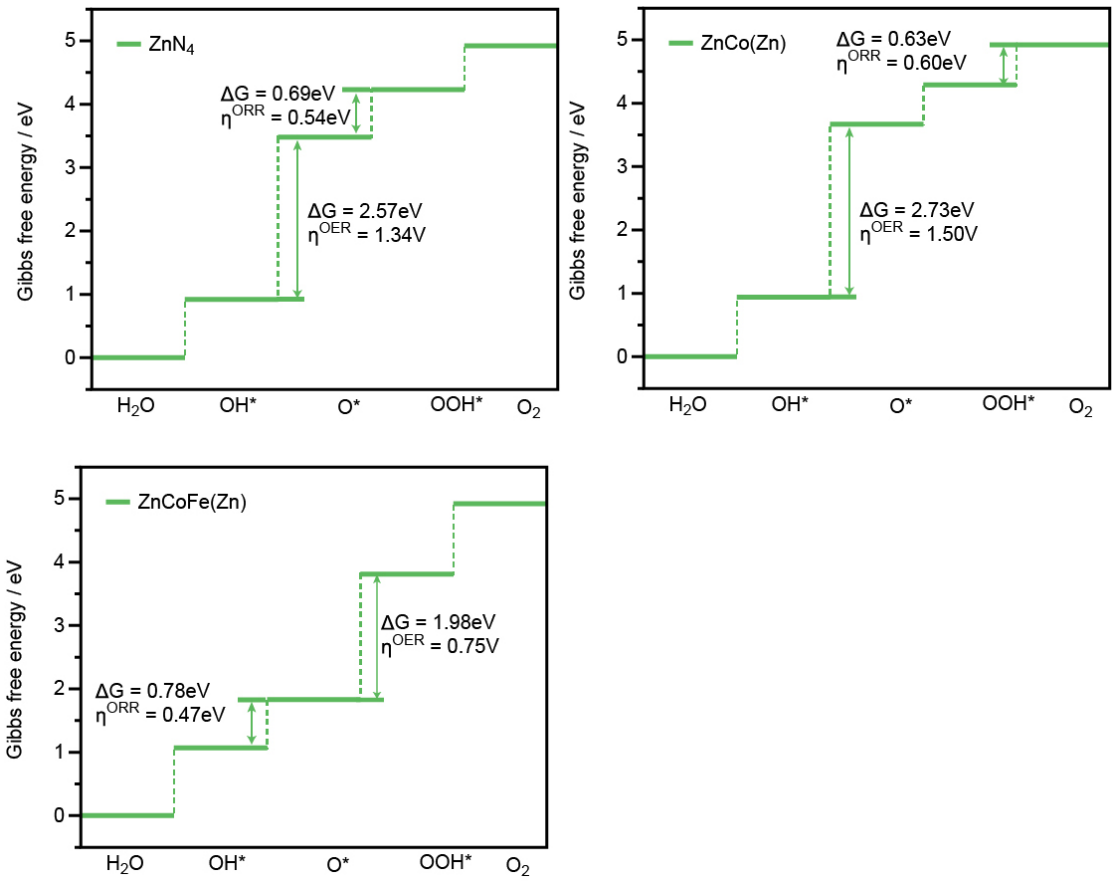

Fig. S34 The free energy diagram (Zn as the active site): (a) ZnN_4, (b) CoZn, (c) CoZnFe.

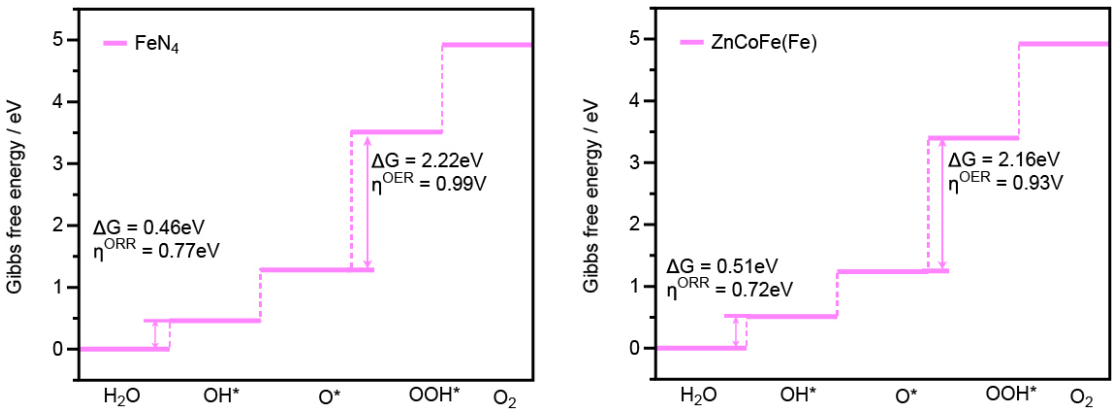

Fig. S35 The free energy diagram (Fe as the active site): (a) FeN_4, (b) CoZnFe.

Tables

Table S1. The contents of the metal element corresponding to the ICP-OES results.

Catalysts	Zn (wt%)	Co (wt%)	Fe (wt%)
Zn/NC	0.15	-	-
ZnCo-DAC/NC	0.17	0.4483	-
ZnCoFe-TAC/NC	0.23	0.39	0.35
ZnCoFe-TAC/SNC	**0.81**	**0.73**	**0.75**

Table S2. BET specific surface areas of all compared samples

Catalysts	BET surface area ($m^2\ g^{-1}$)
Zn/NC	927.56
ZnCo-DAC/NC	1226.80
ZnCoFe-TAC/NC	696.31
ZnCoFe-TAC/SNC	**933.14**

Table S3. The XPS diagram shows the content of elements in ZnCoFe-TAC/SNC.

Name	Peak BE	FWHM eV	Atomic %
S2p	163.77	1.99	1.16
C1s	284.48	1.39	84.54
N1s	398.85	3.63	5.13
O1s	531.45	3.09	7.84
Fe2p	711.05	0.29	0.4
Co2p	780.85	0.21	0.23
Zn2p	1021.33	1.34	0.71

Table S4. Structural parameters extracted from the Fe, Co and Zn K-edge EXAFS fitting. (S_0^2=0.87 for Fe, S_0^2=0.83 for Co, S_0^2=0.85 for Zn)

Sample	Scattering pair	CN	R(Å)	σ^2(10^{-3}Å^2)	ΔE_0(eV)	R factor
FeCoZn-TAC	Fe-N	2.2	1.95	4.5	0.5	0.007
	Fe-S	0.9	2.35	4.9	0.5	
Fe foil	$Fe-Fe_1$	8*	2.47	5.1	1.0	0.005
	$Fe-Fe_2$	6*	2.84	5.4	1.0	
FeCoZn-TAC	$Co-N_1$	1.8	1.93	5.7	-1.5	0.005
	$Co-N_2$	1.9	1.97	6.3	-1.5	
Co foil	Co-Co	12*	2.50	4.6	0.5	0.004
FeCoZn-TAC	$Zn-N_1$	2.0	1.95	6.1	2.0	0.007
	$Zn-N_2$	1.8	2.00	6.7	2.0	
Zn foil	Zn-Zn	12*	2.52	5.4	1.5	0.006

S_0^2 is the amplitude reduction factor; CN is the coordination number; R is interatomic distance (the bond length between central atoms and surrounding coordination atoms); σ^2 is Debye-Waller factor (a measure of thermal and static disorder in absorber-scatterer distances); ΔE_0 is edge-energy shift (the difference between the zero kinetic energy value of the sample and that of the theoretical model). R factor is used to value the goodness of the fitting. Error bounds that characterize the structural parameters obtained by EXAFS spectroscopy were estimated as N ± 20%; R ± 1%; σ^2 ± 20%; ΔE_0 ± 20%.

* This value was fixed during EXAFS fitting, based on the known structure of Fe foil, Co foil and Zn foil.

Table S5. Comparison of bifunctional ORR/OER electrocatalyst in alkaline media.

No.	Catalysts	$E_{1/2(ORR)}$	$\eta_{10(OER)}$ (mV)	ΔE (E_{OER}-E_{ORR})	Ref.
1	NiFe MOF	0.83	300	0.7	[9]
2	N-GRW	0.84	360	0.82	[10]
3	Li_2RuO_3	0.92	340	0.65	[11]
4	NCN-1000-5	0.82	410	0.81	[12]
5	W_2N/WC	0.81	320	0.74	[13]
6	MCN	0.8	421	0.85	[14]
7	Co/CNFs (1000)	0.896	320	0.627	[15]
8	Fe_3C-Co/NC	0.885	340	0.685	[16]
9	S-GNS/NiCo2S4	0.89	330	0.68	[17]
10	Co/N-C	0.896	370	0.704	[18]
11	$Mn_{0.5}(Fe_{0.3}Ni_{0.7})_{0.5}O_x$	0.82	320	0.73	[19]
12	Fe/Co-N-C	0.86	340	0.71	[20]
13	MO-Co@N-C	0.98	390	0.78	[21]
14	NiFe@C@Co	0.87	370	0.749	[22]
15	$Co_3FeS_{1.5}(OH)_6$	0.721	0.358	0.867	[23]
16	Co-Nx-C	0.83	470	0.87	[24]
17	ZnCoFe-TAC/SNC	0.901	347	0.676	This work

Table S6. The calculated zero-point energy and entropy correction values.

Sample	Intermediates	TS/eV	ZPE/eV	G/eV
ZnCoFe	OH*	0.103	0.346	0.299
	O*	0.069	0.062	0.031
	OOH*	0.135	0.433	0.369
CoN_4	OH*	0.100	0.317	0.266
	O*	0.038	0.051	0.033
	OOH*	0.151	0.429	0.353

Table S7. The Gibbs free energy of different intermediates (OH*, O*, and OOH*) in the ORR or OER process.

G/ eV	OH*	O*	OOH*
CoN_4	0.759	2.489	3.792
ZnN_4	0.918	3.484	4.234
FeN_4	0.464	1.284	3.506
CoZn(Co)	0.644	2.132	3.785
CoZn(Zn)	0.941	3.667	4.294
CoFe(Co)	0.994	2.571	3.849
CoZnFe(Co)	0.835	2.366	3.879
CoZnFe(Zn)	1.069	1.826	3.810
CoZnFe(Fe)	0.510	1.238	3.397
CoCoFe(Co)	0.843	2.367	3.619

Reference

1. J. H. G. Kresse *Phys. Rev. B*, 1995, **192**, 222-229.
2. J. F. G. Kresse *Comp. Mater. Sci.*, 1996, **6**, 15-50.
3. G. Kresse, Joubert, D, *Phys. Rev. B*, 1999, **59**, 1758-1775.
4. J. P. Perdew, Burke, K., Ernzerhof, M, *Phys. Rev. Lett.*, 1996, **77**, 3865-3868.
5. H. J. Monkhorst, Pack, J. D. , *Phys. Rev. B*, **13**, 5188-5192.
6. R. Nelson, C. Ertural, J. George, V. L. Deringer, G. Hautier and R. Dronskowski, *J. Comput. Chem.*, 2020, **41**, 1931-1940.
7. S. Maintz, V. L. Deringer, A. L. Tchougréeff and R. Dronskowski, *J. Comput. Chem.*, 2013, **34**, 2557-2567.
8. R. Dronskowski and P. E. Bloechl, *J. Phys. Chem. C*, 1993, **97**, 8617-8624.
9. W. Cheng, X. Zhao, H. Su, F. Tang, W. Che, H. Zhang and Q. Liu, *Nat. Energy*, 2019, **4**, 115-122.
10. H. B. Yang, J. Miao, S.-F. Hung, J. Chen, H. B. Tao, X. Wang, L. Zhang, R. Chen, J. Gao, H. M. Chen, L. Dai and B. Liu, *Sci. Adv.*, 2016, **2**, e1501122.
11. H. Jang, W. Jin, G. Nam, Y. Yoo, J. S. Jeon, J. Park, M. G. Kim and J. Cho, *Energy Environ. Sci.*, 2020, **13**, 2167-2177.
12. H. Jiang, J. Gu, X. Zheng, M. Liu, X. Qiu, L. Wang, W. Li, Z. Chen, X. Ji and J. Li, *Energy Environ. Sci.*, 2019, **12**, 322-333.
13. J. Diao, Y. Qiu, S. Liu, W. Wang, K. Chen, H. Li, W. Yuan, Y. Qu and X. Guo, *Adv. Mater.*, 2020, **32**, 1905679.
14. J. Yan, Y. Wang, Y. Zhang, S. Xia, J. Yu and B. Ding, *Adv. Mater.*, 2021, **33**, 2007525.
15. Z. Yang, C. Zhao, Y. Qu, H. Zhou, F. Zhou, J. Wang, Y. Wu and Y. Li, *Adv. Mater.*, 2019, **31**, 1808043.
16. C. Yang, S. Zai, Y. Zhou, L. Du and Q. Jiang, *Adv. Funct. Mater.*, 2019, **29**, 1901949.
17. W. Liu, J. Zhang, Z. Bai, G. Jiang, M. Li, K. Feng, L. Yang, Y. Ding, T. Yu, Z. Chen and A. Yu, *Adv. Funct. Mater.*, 2018, **28**, 1706675.
18. T. Zhou, W. Xu, N. Zhang, Z. Du, C. Zhong, W. Yan, H. Ju, W. Chu, H. Jiang, C. Wu and Y. Xie, *Adv. Mater.*, 2019, **31**, 1807468.
19. D. M. Morales, M. A. Kazakova, S. Dieckhöfer, A. G. Selyutin, G. V. Golubtsov, W. Schuhmann and J. Masa, *Adv. Funct. Mater.*, 2020, **30**, 1905992.
20. J. Yang, X. Wang, B. Li, L. Ma, L. Shi, Y. Xiong and H. Xu, *Adv. Funct. Mater.*, 2017, **27**, 1606497.
21. B. Chen, X. He, F. Yin, H. Wang, D.-J. Liu, R. Shi, J. Chen and H. Yin, *Adv. Funct. Mater.*, 2017, **27**, 1700795.
22. X. Chen, J. Pu, X. Hu, Y. Yao, Y. Dou, J. Jiang and W. Zhang, *Small*, 2022, **18**, 2200578.
23. H.-F. Wang, C. Tang, B. Wang, B.-Q. Li and Q. Zhang, *Adv. Mater.*, 2017, **29**, 1702327.
24. B.-Q. Li, C.-X. Zhao, S. Chen, J.-N. Liu, X. Chen, L. Song and Q. Zhang, *Adv. Mater.*, 2019, **31**, 1900592.